

Liquid immiscibility between silicate, carbonate and sulfide melts in melt inclusions hosted in co-precipitated minerals from Kerimasi volcano (Tanzania): evolution of carbonated nephelinitic magma

Tibor Guzmics · Roger H. Mitchell ·
Csaba Szabó · Márta Berkesi · Ralf Milke ·
Kitti Ratter

Received: 26 July 2011 / Accepted: 6 February 2012
© Springer-Verlag 2012

Abstract The evolution of a carbonated nephelinitic magma can be followed by the study of a statistically significant number of melt inclusions, entrapped in co-precipitated perovskite, nepheline and magnetite in a clinopyroxene- and nepheline-rich rock (afrikandite) from Kerimasi volcano (Tanzania). Temperatures are estimated to be 1,100°C for the early stage of the melt evolution of the magma, which formed the rock. During evolution, the magma became enriched in CaO, depleted in SiO₂ and Al₂O₃, resulting in immiscibility at ~1,050°C and crustal pressures (0.5–1 GPa) with the formation of three fluid-saturated melts: an alkali- and MgO-bearing, CaO- and FeO-rich silicate melt; an alkali- and F-bearing, CaO- and

P₂O₅-rich carbonate melt; and a Cu–Fe sulfide melt. The sulfide and the carbonate melt could be physically separated from their silicate parent and form a Cu–Fe–S ore and a carbonatite rock. The separated carbonate melt could initially crystallize calciocarbonatite and ultimately become alkali rich in composition and similar to natrocarbonatite, demonstrating an evolution from nephelinite to natrocarbonatite through Ca-rich carbonatite magma. The distribution of major elements between perovskite-hosted coexisting immiscible silicate and carbonate melts shows strong partitioning of Ca, P and F relative to Fe_T, Si, Al, Mn, Ti and Mg in the carbonate melt, suggesting that immiscibility occurred at crustal pressures and plays a significant role in explaining the dominance of calciocarbonatites (sövites) relative to dolomitic or sideritic carbonatites. Our data suggest that Cu–Fe–S compositions are characteristic of immiscible sulfide melts originating from the parental silicate melts of alkaline silicate–carbonatite complexes.

Communicated by J. L. R. Touret.

Electronic supplementary material The online version of this article (doi:10.1007/s00410-012-0728-6) contains supplementary material, which is available to authorized users.

T. Guzmics (✉) · C. Szabó (✉) · M. Berkesi
Lithosphere Fluid Research Laboratory, Institute of Geography
and Earth Sciences, Eötvös University Budapest, Pázmány P.
sétány 1/C, Budapest 1117, Hungary
e-mail: tibor.guzmics@gmail.com

C. Szabó
e-mail: cszabo@elte.hu

R. H. Mitchell
Lakehead University, Thunder Bay, ON P7B 5E1, Canada

R. Milke
Free University Berlin, Habelschwerdter Allee 45, 14195 Berlin,
Germany

K. Ratter
Material Science and Biological Research Center, Eötvös
University Budapest, Pázmány P. sétány 1/C, Budapest 1117,
Hungary

Keywords Melt inclusion · Liquid immiscibility ·
Carbonate melt · Sulfide melt · Silicate melt · Carbonatite ·
Natrocarbonatite · Nephelinite · Kerimasi · Tanzania

Introduction

Carbonatite and associated alkaline silicate rocks occur in numerous igneous complexes (Wooley and Kjarsgaard 2008). Knowledge of the composition and evolution of the primary magma(s) responsible for their crystallization is essential in understanding their petrogenesis. The study of primary melt inclusions is a powerful tool to determine such melt compositions (Le Bas and Aspden 1981; Roedder 1987; Veksler and Lentz 2006; Solovova et al. 2006;

Guzmics et al. 2008, 2011; Mitchell 2009; Panina and Stoppa 2009). These melt inclusion studies and those of natural examples (Le Bas 1977; Nielsen 1980; Hay 1983; Kogarko et al. 1991; Dawson et al. 1994; Mitchell 2005) together with numerous experimental studies (Koster van Groos and Wyllie 1968; Hamilton et al. 1979; Kjarsgaard and Peterson 1991; Lee and Wyllie 1997, 1998; Brooker and Kjarsgaard 2010) suggest that liquid immiscibility might play a major role in the formation of carbonatites. Although different evolutionary paths of the parental melt(s) of alkaline silicate and carbonatite rocks have been suggested (Le Bas 1977; Bailey 1993; Dawson et al. 1996; Nielsen et al. 1997; Lee and Wyllie 1997; Kjarsgaard 1998; Mitchell 2009; Guzmics et al. 2011), several questions remain unanswered.

In this study, we present statistically significant compositional data for primary silicate, silicate–carbonate, and silicate–carbonate–sulfide melt inclusions hosted by co-precipitated nepheline, perovskite and magnetite from a clinopyroxene–nepheline–perovskite–magnetite–melilite rock (afrikandite) collected at Kerimasi Volcano, Tanzania. The melt inclusions show that during evolution of carbonated nephelinite magma, its composition reaches the immiscibility field, resulting in three immiscible melts. To the best of our knowledge, this is the first study reporting immiscibility between silicate, carbonate and sulfide melts. The carbonate melt formed at this time could become the parental melt of calciocarbonatite found at Kerimasi (Guzmics et al. 2011) and other localities (Wooley and Kjarsgaard 2008).

Additionally, we determined the partitioning of major elements in coexisting silicate and carbonate melts in perovskite-hosted melt inclusions to explain the dominance of calciocarbonatites (sövitites) relative to dolomitic or sideritic types (Heinrich 1966; Tuttle and Gittins 1966; Le Bas 1977; Bell 1989).

Sampling and petrography

Samples of 5–8 cm blocks of afrikandite were collected from the major debris flow emanating from Kerimasi volcano at Trig Point Hill. These plutonic rocks have typical igneous texture (Fig. 1a–e) and consist mainly of anhedral (100–500 µm) and subhedral-to-euhedral clinopyroxene together with anhedral nepheline (80–400 µm). Lesser amounts of subhedral-to-euhedral perovskite (100–600 µm), anhedral magnetite (100–300 µm) and anhedral melilite (100–400 µm) also occur. Accessory minerals in the rock are apatite and calcite. The subhedral-to-euhedral clinopyroxenes are megacrysts (2,000–7,000 µm) with a brown core (500–3,000 µm) and a pale green rim (1,000–4,000 µm, Fig. 1c). Anhedral clinopyroxene (= matrix clinopyroxene) is

green and similar to rims of megacrysts (Fig. 1a, b, d). Calcite occurs in clinopyroxenes as inclusions coexisting with perovskite and magnetite (Fig. 1f).

Almost all rock-forming minerals in the afrikandite contain crystalline inclusions of the other rock-forming minerals (for example, green clinopyroxene contains inclusions of magnetite, perovskite and nepheline). Exceptions are the brown cores of clinopyroxene megacrysts that contain only perovskite (50–150 µm, Fig. 1c) and olivine (40–60 µm, Fig. 2a), and magnetite-free perovskite.

Primary, randomly distributed and irregular-shaped melt inclusions occur in perovskite (5–40 µm, Figs. 1d, 2b, c), magnetite (20–40 µm), nepheline (2–50 µm, Fig. 3) and green clinopyroxene (5–30 µm). The melt inclusions contain no bubbles. However, holes (Fig. 2b, c) representing the places of former fluid phase (probably existed inside the melt inclusion before exposure) occur in the melt inclusions. The number of melt inclusions is the greatest in perovskite (Fig. 1d); for example, at least 20 melt inclusions can be found in a 200 × 200 µm area on an exposed surface (Fig. 2b). Several melt inclusions in perovskite have three major parts (crystallized former melt phases): silicate, carbonate and sulfide (Fig. 2b, c). The relative portion of these varies significantly among melt inclusions. High-resolution SE images show that the silicate-rich part of the inclusions consists of 400–600-nm-sized crystals of clinopyroxene and nepheline (dark crystals, Fig. 2c) and matrix. The latter is Fe-rich glass (Fig. 2c). The carbonate-rich fraction consists of alkali carbonates and calcite together with daughter crystals of subhedral apatite (Fig. 2c). The Fe and Cu contents of the sulfides (Fig. 2b, c) vary significantly; no other cations were detected by EDS methods. Clinopyroxene and nepheline are found as heterogeneously entrapped crystals in perovskite-hosted melt inclusions. In the majority of the silicate melt inclusions in perovskite, discrete carbonate- and sulfide-rich parts were not observed. In nepheline, the primary silicate melt inclusions contain Fe-rich silicate glass, together with calcite, magnetite and clinopyroxene as daughter phases. The latter could additionally be found as heterogeneously entrapped crystals. Sulfides rarely occur in nepheline-hosted melt inclusions. Magnetite-hosted melt inclusions are similar to those hosted by perovskite; however, sulfide-rich parts were not found as commonly as in perovskite.

Experimental and analytical methods

For high-resolution BSE (back-scattered electron) and SE (secondary electron) imaging, phase identification and qualitative analysis, we used a FEI QUANTA 3D FIB-SEM instrument equipped with silicon drift energy dispersive spectrometer (EDS) located at Material Science

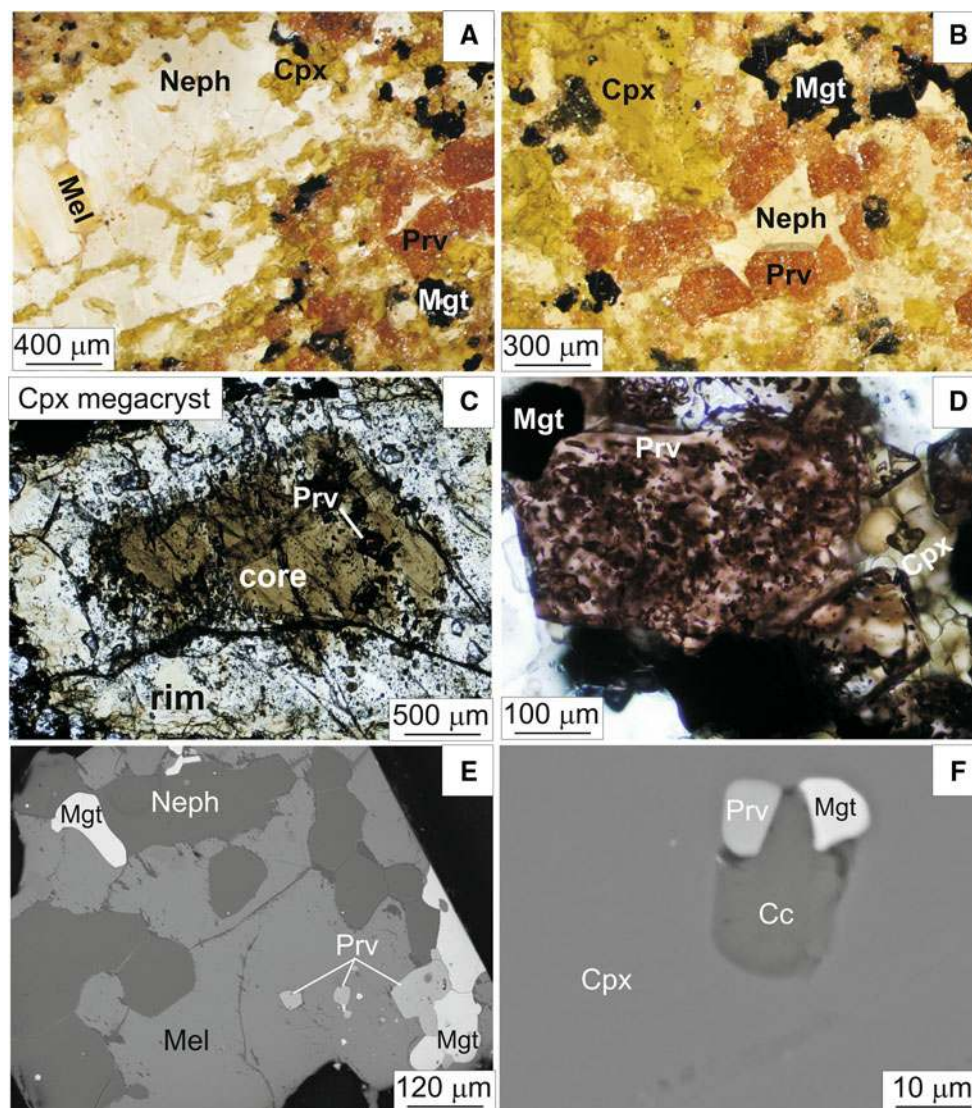


Fig. 1 Petrography and texture of Kerimasi afrikandite. *Cpx* clinopyroxene, *Cc* calcite, *Mel* melilite, *Mgt* magnetite, *Neph* nepheline, *Prv* perovskite. **a–d**—photomicrographs, **e–f**—back-scattered electron

images. It can be seen on picture **d** that perovskite is full of with melt inclusions

and Biological Research Center of Eötvös University and an AMRAY-1830 IT-6 scanning electron microscope located at Department of Petrology and Geochemistry of Eötvös University. Both instruments were operated at 15–20 kV and 0.5–2 nA. Microthermometric experiments were undertaken in the Lithosphere Fluid Research Laboratory, Eötvös University, Budapest, on nepheline-, clinopyroxene- and perovskite-hosted melt inclusions using a Linkam TS 1500 high-temperature stage mounted on a Nikon Eclipse E600 polarization microscope. Heating temperatures ranged between 1,040 and 1,200°C. A furnace technique, using a Carl-Zeiss Jena high-temperature furnace in Lithosphere Fluid Research Laboratory, Eötvös University Budapest, was applied to a significant number of separated perovskite, magnetite and nepheline grains

encapsulated in graphite containers to prevent oxidation during heating–quenching experiments. Temperature used in the experiments for different runs was 1,050°C, with an uncertainty of 15°C. Homogenous melts in the inclusions were produced with a quenching rate of 300–350°C/s. To expose the melt inclusions, all samples were polished on dry Al_2O_3 powder without using any water or oil in the Lithosphere Fluid Research Laboratory, Eötvös University, Budapest. The compositions of rock-forming mineral phases (clinopyroxene, nepheline, perovskite, magnetite and melilite) together with the quenched melt phases inside melt inclusions were determined using a JEOL JXA 8200 Superprobe with five crystal wavelength dispersive spectrometers at the Free University, Berlin. Minerals and quenched sulfide melts were analyzed using 1–2 μm beam,

whereas quenched silicate and carbonate melts were analyzed using a 2–3 μm beam diameter, depending on the measurable area of quenched melts. To minimize error derived from sodium volatilization, this element was analyzed in the first 5 s of the analysis. Accelerating voltage and beam current were 15 kV and 20 nA, respectively.

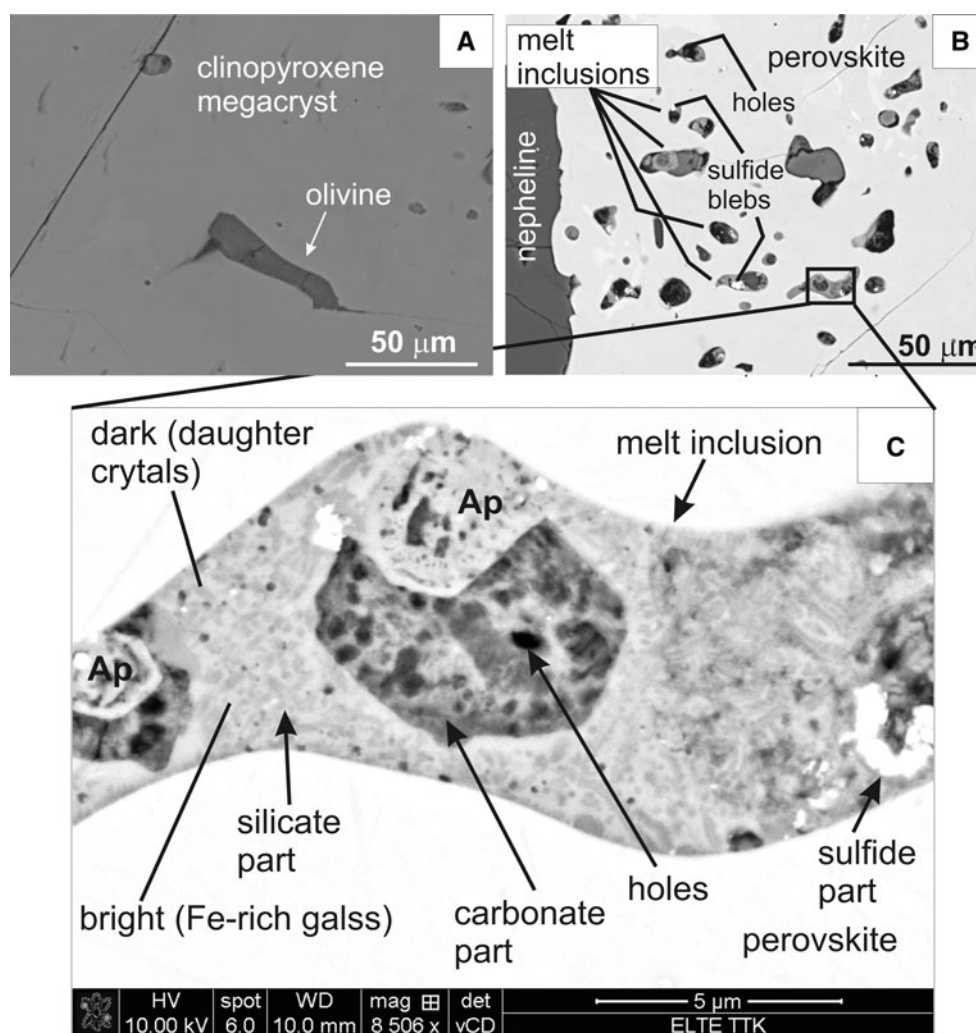
Microthermometry

Microthermometric experiments were carried out on a statistically significant number of nepheline-, perovskite- and clinopyroxene-hosted melt inclusions. During microthermometry, besides the melting of the daughter phases, volatiles incorporated in the daughter phases (e.g., in different carbonates, Fig. 2c) and can be liberated to form a fluid bubble. This fluid bubble can be homogenized into the melt phase. This study, however, does not attempt to deal with composition of the fluid coexisting with melts as these data will be published subsequently.

In general, the majority of melt inclusions investigated could not be homogenized and decrepitated above 1,070°C (clinopyroxene-hosted ones) and 1,180°C (nepheline- and perovskite-hosted ones). However, several melt–fluid homogenizations (into the melt phase) were detected in the inclusions of clinopyroxene (minimum homogenization temperature was 1,040°C) and nepheline (minimum homogenization temperature was 1,050°C). Melting of the last solid daughter phase was observed between 1,040 and 1,050°C, but always before melt–fluid homogenization.

Figure 3 illustrates the major steps in a representative microthermometric experiment on a 20- μm nepheline-hosted silicate melt inclusion. At about 790°C, visible melting commences. At 885°C, the fluid phase formed a globular shape in the melt phase (Fig. 3b). At 957°C, the size of the fluid phase was significantly reduced, and the solid phase(s) still exist(s) (Fig. 3c). At 1,042°C, the last daughter phase (clinopyroxene) melted. At 1,050°C, the melt inclusion showed a negative crystal shape (Fig. 3d).

Fig. 2 Petrography of crystal and melt inclusions in Kerimasi afrikandite, Tanzania. Ap apatite. **a**, **b**—back-scattered electron images, **c**—secondary electron image. Black areas represent places of former fluid phase exists inside the melt inclusions before exposure



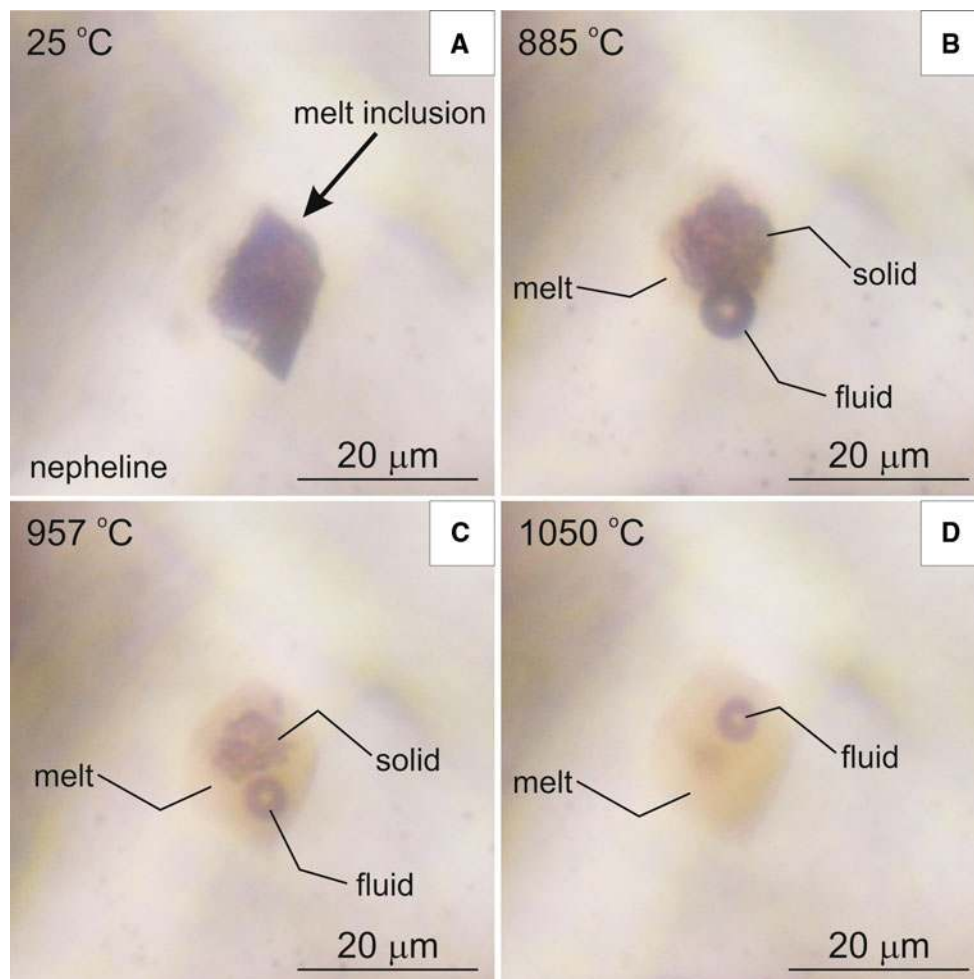


Fig. 3 A representative microthermometric experiment of a nepheline-hosted silicate melt inclusion in Kerimasi afrikandite, Tanzania. Photomicrographs

In this example on further heating, the size of the fluid phase did not decrease significantly; however, visible melting of the wall of the melt inclusion started at 1,120°C.

Heating–quenching experiments and run products

On the basis of the minimum homogenization temperatures observed in our microthermometric experiments, heating–quenching experiments were carried out on nepheline-, magnetite- and perovskite-hosted melt inclusions to reproduce the melt phases at the time of entrapment. The separated grains were heated to 1,050°C and then quenched. Figures 4 and 5 show the quenched melt inclusions in perovskite, magnetite and nepheline. Overall, more than 200 exposed melt inclusions were studied in detail. Typically, in perovskite-hosted melt inclusions the quench products are three immiscible melt phases, that is, silicate, carbonate and sulfide melt with a coexisting fluid bubble (Figs. 4, 5a, b). In many other examples, silicate melt inclusions contain no immiscible carbonate and sulfide

melt phases (Fig. 4d). A silicate melt phase is always present in all melt inclusions and wets the perovskite, including carbonate-rich melt inclusions (Fig. 5b). Carbonate and sulfide melts formed inside the silicate melt and have globular shapes (Figs. 4, 5a, b). When sulfide and carbonate melts are attached, their spherical shapes are deformed such that either the carbonate melt (Figs. 4a, 5a) or the sulfide melt (Fig. 4b) forms a concave surface along their boundary. A fluid bubble is present in the carbonate melt phase (Figs. 4e, f, 5a, b); however, it also occurs in silicate melt phase in inclusions lacking carbonate melt phase (Fig. 4d). The silicate melt phase typically contains 100–300-nm-large quench carbonate melt globules (e.g., Fig. 5a). In a few examples, not completely melted nepheline (Fig. 4d) and clinopyroxene (not shown) crystals are present in perovskite-hosted melt inclusions. The quenched magnetite-hosted melt inclusions show very similar features to those hosted in perovskite (Fig. 5c). For example, immiscible carbonate melts usually are present, although sulfide melts are rarely detected. Quenched nepheline-

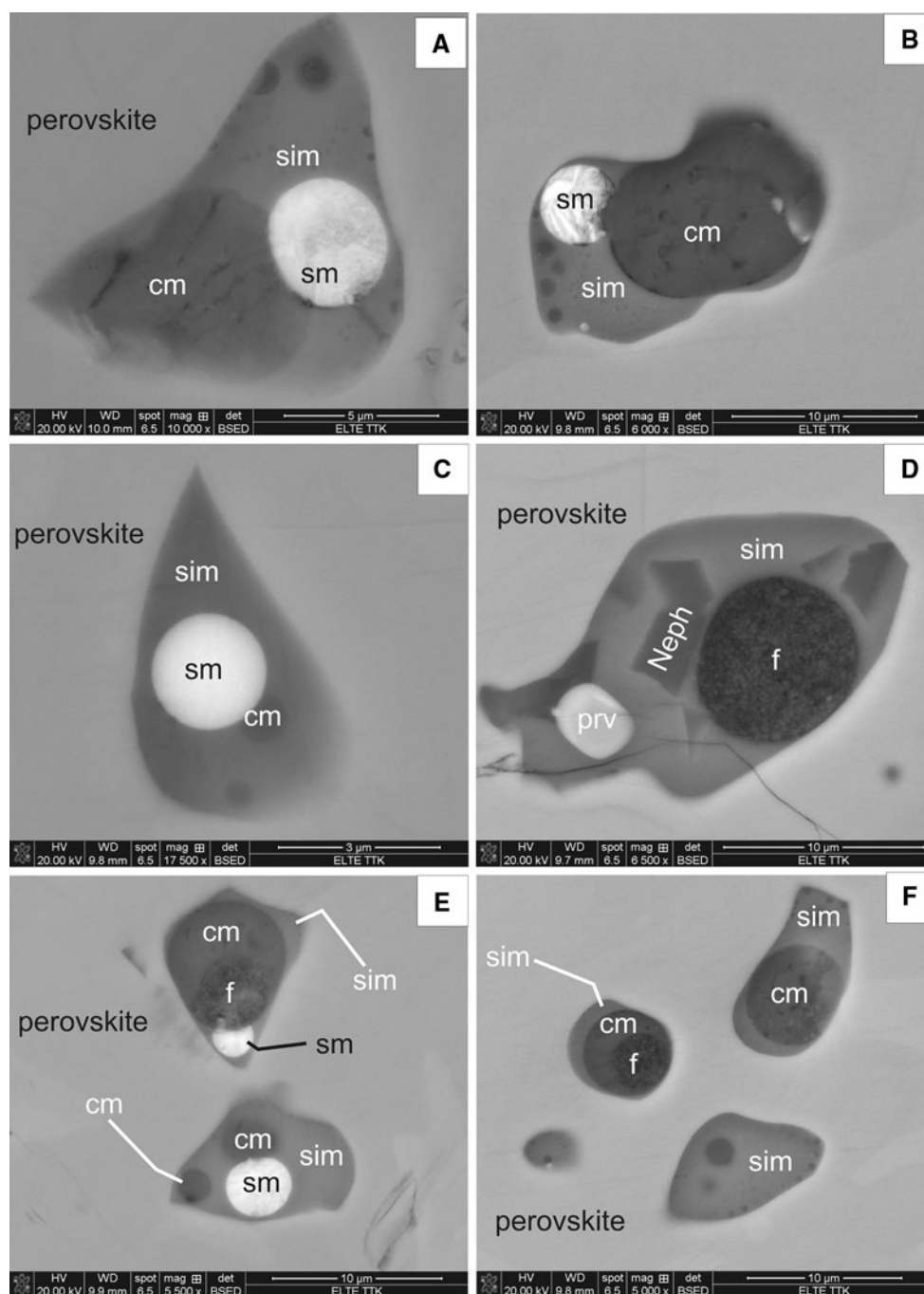


Fig. 4 Representative quenched, perovskite-hosted melt inclusions after heating to 1,050°C. Back-scattered electron images. Hole represents former fluid phase (f) that existed in the inclusions prior to exposure. *Neph* nepheline, *cm* carbonate melt, *sim* silicate melt, *sm* sulfide melt

hosted melt inclusions contain silicate melt, a fluid bubble, but no carbonate melt (Fig. 5d). Rarely, not totally melted clinopyroxenes were found in nepheline-hosted melt inclusions (Fig. 5e). Two textural variations were observed in the quenched sulfide melts: one containing Cu-rich exsolution lamellae (Fig. 4b) and the other being homogeneous in composition (Fig. 4c).

Major element compositions

The rock-forming minerals

Compositions of all analyzed clinopyroxenes are given in Tables 1 and 2. Brown cores of clinopyroxene megacrysts have high Al_2O_3 and TiO_2 contents (3.4–5.6

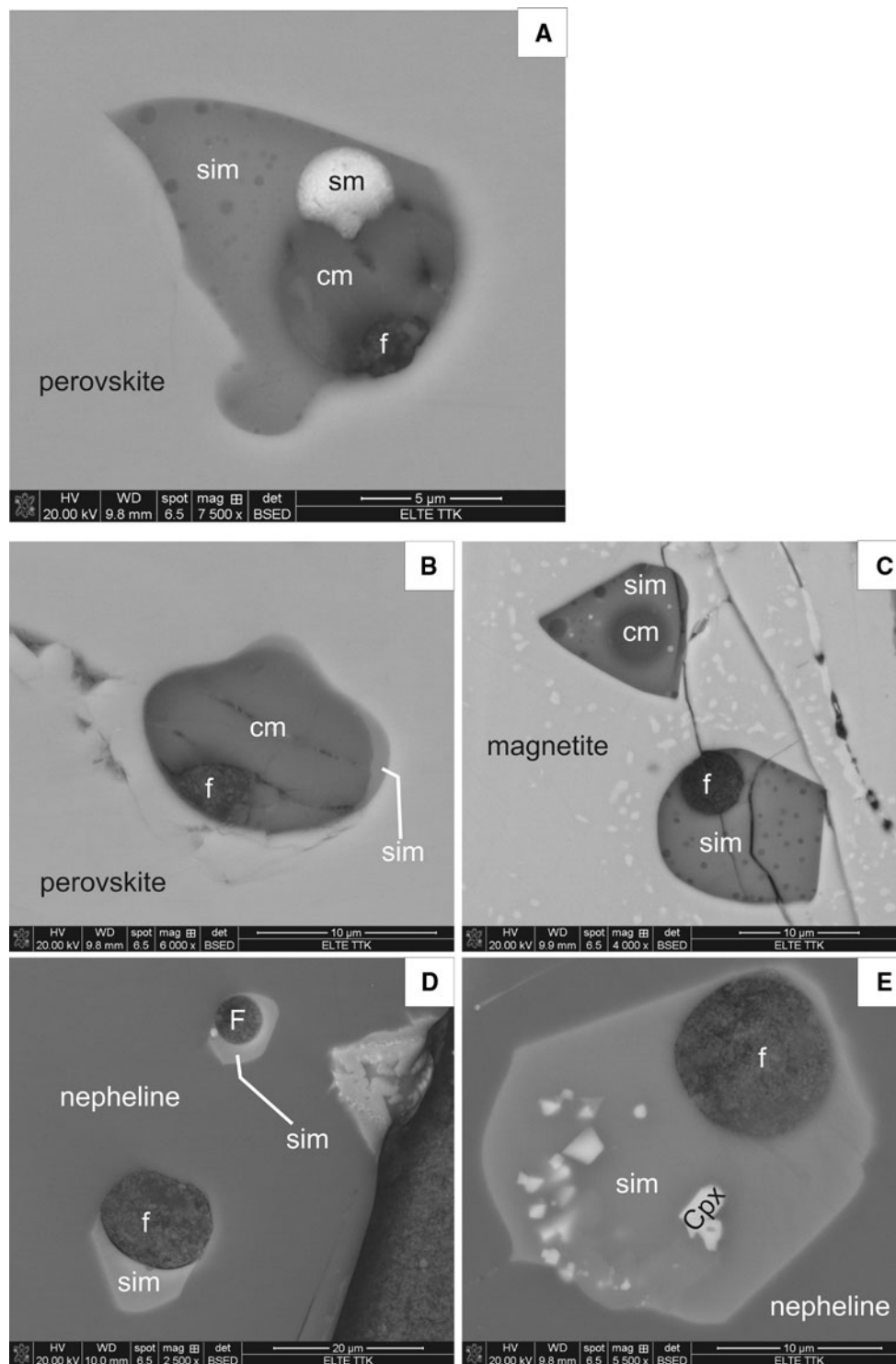


Fig. 5 Representative quenched perovskite-, magnetite- and nepheline-hosted melt inclusions after heating to 1,050°C. Back-scattered electron images. Hole represents former fluid phase (f) that existed in

and 1.8–2.2 wt. %) and have lower SiO₂ contents (47.6–50.2 wt. %) than the green rims and matrix clinopyroxenes (0.3–2.5 Al₂O₃, 0.2–1.2 TiO₂, 50.8–54.5 SiO₂ wt. %, Fig. 6a). MgO varies positively with SiO₂; the

the inclusions prior to exposure. *cm* carbonate melt, *sim* silicate melt, *sm* sulfide melt

concentration ranging from 13.0 to 14.0 wt. % for the brown core of the megacrysts to 14.0–15.5 wt. % in the green rim and matrix clinopyroxenes (Fig. 6b). Compositions of perovskite-hosted inclusions of clinopyroxene

overlap between those of the brown cores of megacrysts and matrix clinopyroxenes (Fig. 6).

Compositions of nepheline are not variable (Table 3), and contain 6.7–7.0 wt. % K_2O , 0.95 wt. % FeO_T and 0.72 wt. % CaO . Perovskite is near-stoichiometric $CaTiO_3$ (Table 4) with minor FeO_T (0.6–1.1 wt. %), Na_2O (0.4 wt. % on average) and BaO (0.3 wt. % on average).

Magnetites are TiO_2 -rich (9.8–10.4 wt. %) and Cr_2O_3 -poor (<0.2 wt. %, Table 5) and are dominantly solid solutions of magnetite (Fe_3O_4), ulvöspinel (Fe_2TiO_4), magnesioferrite ($MgFe_2O_4$), spinel ($MgAl_2O_4$) and jacobsite ($MnFe_2O_4$).

Melilites are of uniform in composition (Table 6) and contain minor K_2O and MnO (0.11 and 0.16 wt. % on average, respectively).

The quenched melts in melt inclusions of perovskite, nepheline and magnetite

Tables 7, 8, 9, 10, 11, 12 and Figs. 7, 8, 9, 10 show the compositions of the quenched melts. The composition of all 153 analyses of quenched melts is given as an electronic

supplement. All silicate and carbonate melts are rich in alkalis ($Na_2O + K_2O$), that is, 6.2–14.5 and 11.5–21.5 wt. %, respectively (Fig. 9).

Silicate melts are rich in FeO_T (8.7–16.6 wt. %), and their compositions vary significantly (Fig. 7). Of significance is the decrease in Al_2O_3 and SiO_2 (from 16.0 to 5.6 wt. % and from 42.9 to 28.5 wt. %, respectively) with increasing of CaO (from 8.1 to 25.0 wt. %) (Fig. 7). Silicate melts coexisting with immiscible carbonate melt (Figs. 4, 5, 7, 9; Table 10) are enriched in CaO and MgO relative to Al_2O_3 and SiO_2 (Figs. 7, 9; Tables 8, 9) in comparison with silicate melts those contain no carbonate melt phase. The majority of the silicate melts contain notable amounts of TiO_2 (1.0–4.7 wt. %), P_2O_5 (0.7–2.7 wt. %) and SO_3 (0.7–1.8 wt. %). The cores of perovskite and some nepheline crystals host MgO - and SiO_2 -rich silicate melt inclusions (Table 7; Figs. 7, 9). These melt inclusions contain neither immiscible carbonate nor sulfide melts.

Overall, the carbonate melts are enriched in alkalis ($Na_2O + K_2O$), CaO (33–43 wt. %), P_2O_5 (3.3–7.3 wt. %), and F (0.7 wt. %, in average), whereas MgO (0.7–2.7 wt.

Table 1 Representative compositions of clinopyroxenes in wt. %. Kerimasi afrikandite, Trig Point Hill, Tanzania

	Matrix (green)										Average $n = 20$	ISD	Rim of megacryst	Inclusion in perovskite		
SiO_2	52.24	51.85	52.78	52.78	52.09	51.60	53.06	54.43	51.88	53.12	52.51	0.83	52.56	50.01	50.45	52.17
TiO_2	0.75	0.83	0.60	0.70	0.73	0.86	0.22	0.34	0.83	0.61	0.69	0.21	0.81	1.35	1.70	0.90
Al_2O_3	1.68	1.97	0.91	1.15	1.33	1.95	0.93	0.37	1.84	0.83	1.32	0.58	1.32	2.95	2.85	1.48
FeO_T	5.85	6.29	6.26	5.59	5.73	6.24	5.56	4.06	6.29	5.12	5.77	0.73	5.25	6.77	6.85	6.10
MnO	0.24	0.29	0.20	0.19	0.43	0.27	0.24	0.31	0.21	0.24	0.25	0.06	0.22	0.26	0.20	0.29
MgO	14.87	14.57	14.83	15.18	14.94	14.41	15.26	15.78	14.77	15.82	15.00	0.51	15.10	14.04	13.93	14.65
CaO	23.44	23.35	23.14	23.37	23.28	23.33	23.42	24.05	23.12	22.98	23.33	0.27	23.71	23.07	23.12	23.60
Na_2O	0.63	0.58	0.65	0.51	0.53	0.61	0.60	0.48	0.48	0.51	0.55	0.06	0.49	0.66	0.66	0.40
Total	99.72	99.75	99.39	99.49	99.14	99.33	99.32	99.83	99.43	99.24			99.52	99.16	99.79	99.69

FeO_T all Fe expressed as FeO , *ISD* one absolute standard deviation

Table 2 Representative compositions of core of clinopyroxene megacryst in wt. %. Kerimasi afrikandite, Trig Point Hill, Tanzania

	Brown core										Average $n = 13$	ISD
SiO_2	48.26		48.47	48.41	47.56	48.56	48.80	48.65	50.19	48.42	0.63	
TiO_2	1.94		1.78	1.87	2.14	1.83	1.80	1.90	1.90	1.85	0.10	
Al_2O_3	5.16		5.02	4.92	5.64	5.04	4.96	4.82	3.41	4.78	0.56	
FeO_T	6.96		6.96	6.96	7.15	6.90	6.87	6.71	6.61	6.86	0.15	
MnO	0.11		0.13	0.14	0.13	0.10	0.10	0.16	0.10	0.13	0.02	
MgO	13.27		13.36	13.24	13.05	13.31	13.21	13.41	13.96	13.44	0.24	
CaO	23.45		23.29	23.34	23.12	23.39	23.41	23.43	22.15	23.23	0.37	
Na_2O	0.55		0.58	0.45	0.59	0.54	0.56	0.60	0.65	0.52	0.05	
Total	99.71		99.68	99.34	99.44	99.69	99.78	99.79	98.99			

FeO_T all Fe expressed as FeO , *ISD* one absolute standard deviation

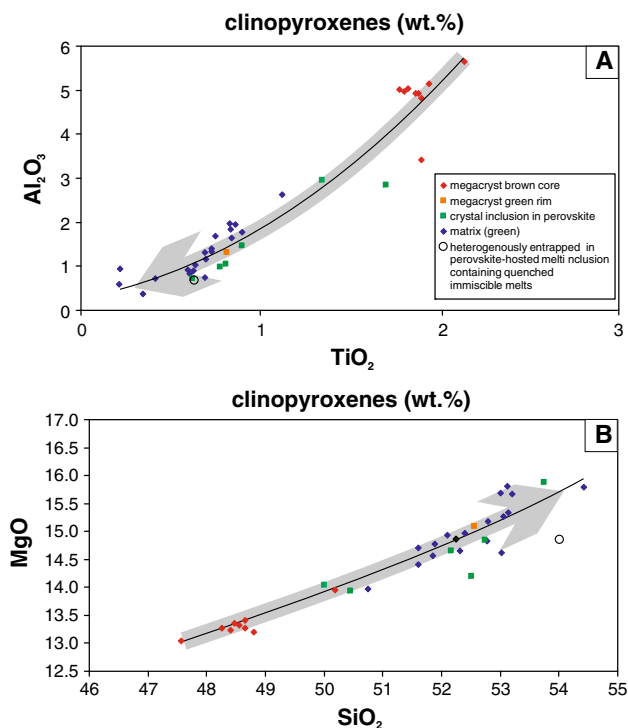


Fig. 6 Compositional variation of clinopyroxenes in Kerimasi afrikandite, Tanzania. *Gray arrow* shows the compositional change of clinopyroxenes with melt evolution

%), FeO_T (0.4–2.8 wt. %) and SiO_2 (1.3–2.2 wt. %) are present in lesser amounts compared to the silicate melts (Tables 10, 12; Fig. 9).

Sulfide melts consist of S, Fe and Cu (Table 11). Copper and iron are significantly, in contrast to S, reflecting changes in composition from Cu-rich melts to those similar

to FeS–Fe binary compositions (through intermediates). Sulfide melts contain very low amounts of Ni (<0.2 wt. %, Table 11).

Discussion

Our study of clinopyroxene- and nepheline-hosted silicate melt inclusions show melting of the last daughter phases between 1,040 and 1,050°C (Fig. 3) and minimum fluid-melt homogenization at 1,040–1,050°C. On the basis of these observations, it is concluded that crystallization of the afrikandite could have happened in the range of 1.050–1.100°C.

Triple melt immiscibility between silicate, carbonate and sulfide melts

Many perovskite-hosted quenched melt inclusions show the coexistence of three immiscible melt phases (silicate, carbonate and sulfide) together with a fluid phase (Figs. 4, 5). During our experiments, the melts in perovskite-hosted melt inclusions never homogenized completely into one melt phase, even when temperatures are increased to 1,180°C. At this temperature, perovskite started melting resulting in decrepitation of melt inclusions at 1,200°C. In the perovskite-hosted quenched melt inclusions, the proportion of the quenched melt phases and fluid phase are highly variable (Figs. 4, 5b). These observations imply that immiscible silicate, carbonate and sulfide melt phases together with a fluid phase coexisted before or during precipitation of such perovskites. Entrapment of the phases in arbitrarily proportions is termed heterogeneous entrapment and has been observed in diverse

Table 3 Representative compositions of nepheline in wt. %. Kerimasi afrikandite, Trig Point Hill, Tanzania

	Rock forming															Inclusions in perovskite	Average (n = 22)	1SD
SiO_2	40.49	40.77	40.57	40.62	40.56	40.55	40.69	40.65	40.67	40.50	40.44	40.60	40.48	40.52	40.59	0.08		
TiO_2	0.02	nd	0.01	nd	0.01	0.02	0.01	nd	0.00	nd	0.01	0.02	0.26	0.12	0.03	0.06		
Al_2O_3	34.56	34.41	34.63	34.41	34.48	34.55	34.61	34.56	34.65	34.66	34.67	34.63	34.73	34.69	34.64	0.12		
FeO_T	1.01	1.11	0.95	1.11	1.10	1.07	1.06	1.03	0.97	0.88	0.92	0.99	0.83	0.87	0.95	0.12		
MnO	0.04	0.01	0.01	nd	nd	nd	0.01	0.00	nd	0.01	0.04	nd	0.00	nd	0.01	0.02		
MgO	0.09	0.07	0.07	0.08	0.07	0.08	0.09	0.07	0.08	0.08	0.07	0.07	0.09	0.08	0.07	0.01		
CaO	0.71	0.70	0.73	0.72	0.73	0.69	0.70	0.72	0.73	0.75	0.75	0.71	0.88	0.74	0.72	0.04		
BaO	0.03	0.02	nd	nd	0.02	0.02	nd	0.05	nd	0.03	0.01	0.02	0.02	0.05	0.02	0.02		
Na_2O	16.07	16.20	16.18	16.12	16.25	16.39	16.27	16.19	16.16	16.19	16.24	16.18	16.01	16.19	16.18	0.09		
K_2O	6.87	6.74	6.86	6.68	6.63	6.61	6.70	6.78	6.77	6.77	6.66	6.81	6.71	6.62	6.76	0.11		
Total	99.89	100.03	100.02	99.76	99.87	99.99	100.16	100.06	100.03	99.87	99.81	100.04	99.89	99.89				
PI	0.98	0.99	0.98	0.98	0.98	0.99	0.98	0.98	0.98	0.98	0.98	0.98	0.97	0.98	0.98	0.00		

FeO_T all Fe expressed as FeO, *1SD* one absolute standard deviation, *nd* not detected, *PI* peralkalinity = $(Na_2O + K_2O)/Al_2O_3$ as molar proportion

Table 4 Representative compositions of perovskite in wt. %. Kerimasi afrikandite, Trig Point Hill, Tanzania

										Average ($n = 20$)	1SD
TiO ₂	57.88	58.65	57.81	58.51	57.94	57.84	58.29	58.31	57.87	58.10	0.42
FeO _T	0.67	0.86	0.78	1.09	0.61	0.58	0.79	0.67	0.60	0.72	0.13
CaO	38.69	38.90	38.96	38.83	38.75	38.62	39.06	38.55	38.45	38.62	0.43
BaO	0.24	0.33	0.37	0.29	0.28	0.28	0.34	0.27	0.27	0.30	0.04
Na ₂ O	0.32	0.34	0.23	0.43	0.44	0.34	0.31	0.32	0.45	0.39	0.12
Total	97.79	99.09	98.14	99.15	98.02	97.66	98.79	98.12	97.64		

FeO_T all Fe expressed as FeO, *ISD* one absolute standard deviation

Table 5 Representative compositions of magnetite in wt. %. Kerimasi afrikandite, Trig Point Hill, Tanzania

										Average ($n = 20$)	1SD
TiO ₂	10.04	9.81	9.97	9.96	10.28	9.86	10.13	10.18	10.27	10.14	0.17
Al ₂ O ₃	1.77	1.79	1.71	1.67	1.66	1.64	1.55	1.69	1.72	1.79	0.11
Cr ₂ O ₃	0.15	0.20	0.19	0.18	0.15	0.10	0.17	0.18	0.22	0.19	0.04
FeO _T	78.58	78.73	78.75	78.94	78.73	79.06	78.94	78.66	78.35	78.55	0.25
MnO	1.22	1.27	1.20	1.23	1.27	1.17	1.22	1.12	1.22	1.25	0.05
MgO	3.31	3.24	3.24	3.08	3.04	3.20	3.08	3.27	3.34	3.20	0.09
Total	95.08	95.04	95.06	95.07	95.12	95.03	95.08	95.10	95.12		

FeO_T all Fe expressed as FeO, *ISD* one absolute standard deviation

Table 6 Representative compositions of melilite in wt. %. Kerimasi afrikandite, Trig Point Hill, Tanzania

										Average ($n = 20$)	1SD
SiO ₂	44.19	44.23	44.21	44.27	44.62	44.48	44.55	44.62	44.46	44.49	0.31
TiO ₂	0.02	0.03	0.04	0.05	0.07	0.06	0.04	0.07	nd	0.04	0.02
Al ₂ O ₃	7.38	7.22	7.02	7.09	7.06	7.34	7.22	7.08	7.46	7.14	0.28
FeO _T	4.39	4.44	4.36	4.49	4.43	4.34	4.30	4.29	4.19	4.36	0.08
MnO	0.16	0.16	0.16	0.16	0.16	0.18	0.16	0.19	0.19	0.16	0.02
MgO	7.10	7.11	7.06	7.20	6.98	7.08	7.06	7.19	7.06	7.10	0.07
CaO	32.34	32.27	32.17	32.12	31.91	31.77	32.02	32.23	31.90	32.01	0.21
BaO	nd	0.04	0.02	nd	nd	0.01	0.03	nd	nd	0.02	0.02
Na ₂ O	4.17	4.35	4.68	4.41	4.42	4.48	4.29	4.15	4.43	4.39	0.14
K ₂ O	0.12	0.10	0.10	0.10	0.10	0.12	0.10	0.10	0.12	0.11	0.01
Total	99.88	99.96	99.84	99.89	99.75	99.87	99.76	99.92	99.82		
PI	0.95	1.01	1.11	1.04	1.04	1.02	0.99	0.98	0.99	1.03	0.05

FeO_T all Fe expressed as FeO, *ISD* one absolute standard deviation, *PI* peralkalinity = $(Na_2O + K_2O)/Al_2O_3$ as molar portion

melt and fluid inclusions (e.g., Roedder 1984, 1987; Danyushkevsky et al. 2002; Bodnar and Student 2006; Veksler 2006; Mitchell 2009; Hidas et al. 2010; Guzmics et al. 2011). Crystals that have been precipitated prior to forming of melt inclusion could also be entrapped heterogeneously. Temperatures of homogenization higher than $\sim 1,050^\circ\text{C}$, microthermometric experiments with decrepitation and not complete melting (during our heating–quenching experiments) of heterogeneously entrapped crystals in the melt inclusions (Figs. 4d, 5e) result from this phenomenon. The melt phases in perovskite (Figs. 4, 5) must have been saturated with

respect to each other and the fluid phase. The presence of 100–200-nm-large carbonate melt droplets exsolved during the quench (Fig. 5a, c) in many silicate melt phases, and the SiO₂ content of the carbonate melt phase (1.3–2.2 wt. %) (Table 8) suggests that they can partially dissolve in each other at 1,050°C. This is supported by similar quench carbonate melt droplets formed in immiscible silicate melts in the experimental run products of Brooker and Kjarsgaard (2010, their Fig. 2).

The S-contents of 3,000–7,000 ppm (Fig. 10) of the silicate melts in perovskite-hosted melt inclusions are

Table 7 Compositions (wt. %) of quenched (after heating to 1,050°C), Mg- and Si-rich silicate melt inclusions hosted in core of perovskite (Prv) and nepheline (Neph). Kerimasi afrikandite, Trig Point Hill, Tanzania

No.	65	117	136	137	138	145	155	3	58	170
Host	Prv	Prv	Prv	Prv	Prv	Prv	Prv	Neph	Neph	Neph
SiO ₂	42.84	41.54	38.60	40.37	41.55	39.63	40.46	40.07	40.33	42.07
TiO ₂	4.69	4.46	4.70	4.22	3.40	4.74	4.71	3.48	3.19	2.26
Al ₂ O ₃	13.21	12.61	16.07	14.03	15.68	14.70	15.44	15.25	14.32	13.53
FeO _T	9.06	8.52	9.50	9.91	11.80	9.86	10.04	7.19	7.55	8.96
MnO	0.24	0.29	0.38	0.37	0.47	0.36	0.33	0.36	0.34	0.43
NiO	0.01	0.01	nd	0.01	nd	0.02	nd	nd	0.02	nd
MgO	5.26	6.33	6.18	5.06	4.88	5.72	5.71	6.38	6.72	5.04
CuO	0.08	0.01	0.04	0.06	0.18	0.02	0.03	0.16	0.06	0.03
CaO	10.39	11.19	10.95	12.08	8.10	11.07	11.00	12.28	12.65	9.70
BaO	0.17	0.03	0.16	0.17	0.16	0.29	0.26	nd	0.06	0.01
Na ₂ O	3.95	5.64	7.49	7.08	6.27	7.61	5.62	5.13	3.44	9.55
K ₂ O	2.21	2.41	3.14	2.82	3.79	3.14	3.28	3.64	3.14	4.90
P ₂ O ₅	1.18	0.87	0.50	0.72	0.46	0.58	0.58	2.18	2.14	0.56
F	0.02	nd	nd	nd	nd	nd	nd	nd	0.07	nd
SO ₃	0.04	0.03	0.04	0.05	0.04	0.06	0.04	0.06	0.04	0.04
Cl	0.01	0.01	0.01	nd	0.01	nd	nd	nd	nd	nd
Total	93.35	93.96	97.76	96.93	96.79	97.80	97.50	96.18	94.07	97.09

nd not detected, FeO_T all Fe expressed as FeO

Table 8 Representative compositions (wt. %) of quenched (after heating to 1,050°C) silicate melts in melt inclusions hosted by perovskite (Prv). Kerimasi afrikandite, Trig Point Hill, Tanzania

No.	7	26	28	31	34	36	40	41	47	56	118	127	174	200	(n = 42)	
															Min	Max
SiO ₂	28.52	30.16	29.17	30.62	30.31	31.45	34.08	35.64	37.71	33.28	29.77	40.61	33.94	35.93	28.52	42.06
TiO ₂	3.84	3.72	3.70	4.00	3.56	3.25	3.45	3.54	3.45	3.00	3.26	4.26	3.52	4.08	2.92	4.76
Al ₂ O ₃	6.38	5.56	6.19	7.51	6.41	7.21	5.98	6.46	11.72	8.54	5.56	9.56	11.10	10.37	5.56	12.15
FeO _T	11.42	10.37	10.95	11.27	10.28	10.55	11.86	12.00	12.03	11.97	11.34	11.86	11.79	9.49	9.49	12.44
MnO	0.88	0.87	1.07	0.80	0.83	0.72	0.84	0.88	0.55	0.79	0.97	0.58	0.62	0.53	0.53	1.07
NiO	nd	0.01	nd	nd	0.02	0.04	0.00	0.01	0.02	nd	0.03	nd	0.04	0.01	–	0.06
MgO	5.08	4.52	5.80	4.52	4.28	4.08	3.39	3.14	3.20	4.22	4.52	3.25	3.38	3.91	2.67	5.80
CuO	nd	0.02	0.03	0.01	nd	nd	nd	nd	0.01	0.01	0.05	nd	0.05	nd	–	0.50
CaO	23.18	25.08	21.84	21.52	20.60	21.15	21.60	18.71	13.69	17.89	23.21	14.04	15.71	17.94	10.86	25.08
BaO	0.21	0.16	0.22	0.15	0.15	0.11	0.09	0.18	0.12	0.12	0.22	0.03	0.14	0.01	0.01	0.22
Na ₂ O	6.99	7.20	8.78	7.78	7.01	7.69	5.49	4.81	7.47	7.49	4.98	4.37	6.44	7.01	4.35	9.92
K ₂ O	2.53	2.10	2.45	2.59	2.61	3.35	2.98	2.62	3.91	2.99	2.17	3.81	3.55	3.29	2.10	4.85
P ₂ O ₅	1.98	2.15	1.82	1.75	1.56	1.86	2.46	2.33	0.77	1.85	2.22	0.92	1.97	2.58	0.63	2.65
F	0.01	nd	nd	nd	nd	nd	nd	nd	0.11	0.10	0.19	nd	0.18	nd	–	0.37
SO ₃	1.26	1.41	1.77	1.42	1.54	1.08	1.33	1.24	0.81	1.21	1.60	0.93	1.14	0.80	0.70	1.77
Cl	0.01	0.01	nd	0.01	0.01	0.02	0.00	0.01	0.01	nd	nd	nd	nd	nd	–	0.03
Total	92.28	93.35	93.78	93.94	89.15	92.57	93.57	91.57	95.59	93.45	90.10	94.21	93.56	95.94		

Note that all of studied quenched silicate melt compositions in perovskite ($n = 42$) can be followed as electronic supplement. nd not detected, FeO_T all Fe expressed as FeO

much higher than those of sulfur-saturated basaltic magma, which are approximately 1,000–2,000 ppm at 1,050°C (Li and Ripley 2005; Liu et al. 2007). However, in silicate

melts the solubility of S increases with increasing FeO, alkalis, CaO content and temperature, coupled with decreasing SiO₂, Al₂O₃, Fe₂O₃ contents and pressure

Table 9 Compositions (wt. %) of quenched (after heating to 1,050°C) silicate melt inclusions hosted in magnetite (Mgt) and nepheline (Neph). Kerimasi afrikandite, Trig Point Hill, Tanzania

No.	158	159	160	164	165	166	167	168	169	170	60	70	74	76	84
Host	Mgt	Mgt	Mgt	Mgt	Mgt	Mgt	Mgt	Mgt	Mgt	Mgt	Neph	Neph	Neph	Neph	Neph
SiO ₂	31.69	31.36	31.93	37.40	32.40	31.77	31.02	32.49	32.13	31.11	41.59	37.74	41.97	38.89	39.62
TiO ₂	3.03	0.96	2.60	3.13	1.30	1.49	2.39	3.35	1.43	1.15	2.88	2.87	1.36	1.22	1.86
Al ₂ O ₃	6.58	6.66	6.01	6.63	7.14	7.45	5.07	6.06	7.70	7.94	14.79	7.18	11.50	8.21	13.22
FeO _T	11.38	13.92	14.03	12.59	14.28	14.40	13.19	14.71	14.53	14.17	8.78	16.66	12.57	14.09	11.85
MnO	0.93	1.20	0.90	0.72	1.09	1.08	0.82	0.91	1.00	1.20	0.34	0.74	0.67	0.71	0.62
NiO	nd	0.04	nd	nd	nd	nd	0.03	nd	nd	0.03	nd	0.04	nd	nd	0.02
MgO	3.48	4.71	3.54	2.68	4.02	4.11	3.15	3.31	4.14	4.84	3.35	3.34	3.14	3.64	3.36
CuO	0.05	0.09	0.01	0.01	0.04	0.03	0.03	0.04	0.04	0.03	0.08	nd	nd	nd	0.03
CaO	22.18	17.76	24.32	16.99	19.05	18.16	23.23	22.26	18.03	16.91	12.18	14.34	12.54	15.62	12.89
BaO	0.02	0.04	nd	0.14	0.10	0.12	0.01	0.09	0.14	nd	0.14	0.17	0.04	0.13	0.06
Na ₂ O	9.11	9.81	6.41	10.90	8.06	8.49	8.01	7.59	8.32	10.62	6.02	6.85	7.75	7.41	9.26
K ₂ O	1.20	2.09	1.00	3.40	1.54	2.02	1.63	0.94	2.02	1.58	2.85	2.86	2.86	2.78	3.09
P ₂ O ₅	0.94	1.47	0.72	1.99	1.41	1.52	1.35	0.69	1.53	1.07	0.60	0.44	0.23	0.70	0.21
F	0.10	0.25	0.16	nd	0.27	0.30	0.31	0.10	0.27	0.21	nd	nd	nd	nd	nd
SO ₃	0.80	1.89	0.69	1.38	1.06	1.42	0.97	0.72	1.64	0.68	0.37	1.10	0.65	1.36	0.60
Cl	0.01	0.02	0.01	0.01	0.01	0.01	0.01	nd	nd	nd	nd	0.01	0.01	nd	0.02
Total	91.50	92.26	92.32	97.97	91.77	92.36	91.20	93.26	92.90	91.51	93.97	94.33	95.28	94.76	96.71

nd not detected, FeO_T all Fe expressed as FeO

(Haughton et al. 1974; Poulson and Ohmoto 1990; Mavrogenes and O'Neil 1999; O'Neil and Mavrogenes 2002; Liu et al. 2007). The perovskite-hosted silicate melts are generally higher in FeO_T (av. 11.2 wt. %), alkalis (Na₂O + K₂O = av. 10.0 wt. %) and CaO (av. 17.0 wt. %) and lower in SiO₂ (av. 34.5 wt. %) and Al₂O₃ (av. 9.5 wt. %) than most basalts. Thus, silicate melts in the melt inclusions can be considered as melts with high S solubility relative to basalts.

Immiscibility between sulfide and basic silicate melts is a well-known phenomenon at crustal pressures (Naldrett 1989; Roedder 1992; Ripley et al. 2002). Kogarko et al. (2001) have described silicate glass, nearly pure calcite globules (without any alkalis) and Fe–Ni sulfides in mantle xenoliths and, on the basis of texture, have interpreted these as representing three immiscible melts. However, as is shown by numerous experiments (Lee and Wyllie 1997, 1998; Kjarsgaard 1998; Brooker and Kjarsgaard 2010) and by natural melt inclusions (e.g., Seifert and Thomas 1995; Nielsen et al. 1997; Sokolov et al. 1999; Rass and Plechov 2000; Mitchell 2009; Guzmics et al. 2011) that globules of calcite or nearly pure calcite (carbonate without alkalis) cannot represent immiscible carbonate melt coexisting with silicate melt as their compositions do not plot in any experimentally constrained immiscibility field. Our melt inclusion data also show (Fig. 9) that significant amounts of alkalis, at least 7–10 wt. % of total Na₂O + K₂O is required to produce silicate–carbonate immiscibility,

regardless of the coexistence of a sulfide melt. In summary, we consider that immiscibility between three fluid-saturated melts (silicate, carbonate and sulfide) occurred during the crystallization of the afrikandite host rock.

Melt(s) evolution based on composition of the quenched melt inclusions

Although the quenched sulfide melts show consistent compositional variations with basalt-coexisted sulfide melts determined experimentally by Ripley et al. (2002), discussion of their compositional evolution is beyond the scope of the present work and will be published subsequently. In this study, we focus on the compositional evolution of the silicate and carbonate melts.

Figure 7 shows the compositional variation of all analyzed quenched silicate melts. The direction of melt evolution during crystallization (Fig. 7a) shows decrease in Al₂O₃ with increase in CaO, indicating nepheline precipitation. However, other Mg- and Si-rich silicate melt inclusions (Fig. 7b), occurring in the cores of perovskite and nepheline (Fig. 7c; Table 7), do not plot on the same trend. To explain the compositional evolution of the melt(s), all the melt compositions ($n = 137$) are plotted on a pseudo-quaternary diagram from haplocarbonatite system [(CaO)–(MgO + FeO_T)–(SiO₂ + Al₂O₃ + TiO₂)–(Na₂O + K₂O)–(CO₂)] (Fig. 9a, b), where 1 GPa experimentally determined (Lee and Wyllie 1998) silicate–carbonate

Table 10 Representative compositions (wt. %) of quenched (after heating to 1,050°C) immiscible silicate and carbonate melts in perovskite-hosted melt inclusions

No.	22	23	49	50	63	64	66	67	68	69	92	93	106	107
	Silicate	Carbonate	Silicate	Carbonate	Carbonate	Silicate	Carbonate	Silicate	Carbonate	Silicate	Carbonate	Silicate	Carbonate	Silicate
SiO ₂	29.65	1.71	31.11	1.54	1.41	29.33	1.82	31.55	2.21	33.30	1.78	29.72	1.30	30.02
TiO ₂	3.83	0.59	3.04	0.63	0.45	3.36	0.44	3.29	0.99	3.05	0.44	3.37	0.48	3.03
Al ₂ O ₃	6.73	0.04	6.66	0.04	0.06	5.67	0.09	5.88	0.05	7.10	0.22	6.83	0.02	6.22
FeO _T	11.85	0.97	11.19	0.74	1.42	11.80	0.68	11.32	1.24	11.63	1.17	11.18	1.27	11.78
MnO	0.89	0.18	0.91	0.22	0.26	0.96	0.11	0.97	0.20	0.82	0.26	0.97	0.23	1.07
NiO	0.02	0.03	nd	nd	0.12	nd	0.04	nd	0.02	0.02	0.03	nd	0.02	0.02
MgO	4.60	1.16	4.58	1.74	1.81	4.80	1.31	4.28	1.00	4.06	1.61	5.70	2.51	5.22
CuO	nd	nd	0.02	0.05	nd	0.03	0.02	0.08	nd	0.01	0.02	nd	nd	0.02
CaO	22.51	38.76	21.54	41.16	38.52	22.44	37.06	21.52	41.28	19.67	41.10	22.88	38.32	22.92
BaO	0.11	0.19	0.07	0.14	1.14	0.10	0.22	0.08	0.10	0.01	0.32	0.16	0.32	0.13
Na ₂ O	7.74	7.69	6.57	8.44	8.20	6.36	11.04	5.66	8.11	5.04	8.27	7.73	10.32	7.32
K ₂ O	2.50	8.15	2.34	4.35	6.39	2.57	7.43	2.19	4.57	2.58	5.24	2.34	5.53	2.61
P ₂ O ₅	2.09	4.48	2.26	4.52	6.27	2.01	4.97	2.28	3.18	2.17	7.71	1.99	5.29	2.12
F	0.09	0.27	0.17	0.81	0.77	0.26	0.34	0.08	0.25	0.08	0.72	0.14	0.99	0.19
SO ₃	1.52	0.13	1.23	0.18	0.38	1.79	0.05	1.10	0.08	1.12	0.10	1.23	0.13	1.51
Cl	nd	0.01	nd	0.01	0.02	0.03	0.01	0.01	nd	0.01	0.01	nd	0.01	nd
Total	94.13	64.36	91.66	64.58	67.23	91.50	65.62	90.31	63.29	90.68	69.00	94.26	66.73	94.17

Kerimasi afrikandite, Trig Point Hill, Tanzania. Compositions of coexisting melts are abreast

Note that compositions of all studied quenched, coexisting silicate and carbonate melt ($n = 26, 13$ pairs) can be followed as electronic supplement. *nd* not detected, FeO_T all Fe expressed as FeO

Table 11 Representative compositions (wt. %) of quenched (after heating to 1,050°C) sulfide melts in melt inclusions hosted in perovskite, Kerimasi afrikandite, Trig Point Hill, Tanzania

No. of coexisting:										
Sulfide melt	7	na	34	41	67	93	107	118		
Carbonate melt	na	16	na	na	66	92	106	na	(n = 15)	
No.	2	5	8	11	14	16	19	22	Min	Max
S	34.37	32.21	29.26	33.92	35.05	33.88	34.03	31.28	20.97	37.04
Cu	13.03	17.79	0.17	23.78	15.93	14.63	8.97	0.08	0.08	69.24
Ni	0.10	0.07	0.04	0.05	0.16	0.01	0.06	0.03	–	0.20
Fe	49.99	46.96	67.02	40.16	44.75	48.47	52.92	65.85	5.75	67.02
Co	0.06	0.02	0.05	0.03	0.05	0.01	0.03	0.05	–	0.07
Total	97.56	97.05	96.53	97.94	95.94	97.00	96.01	97.29		

All the sulfide melt is coexisting with immiscible silicate melt and most of them additionally with carbonate melt

Note that composition of all the studied sulfide melt can be followed as electronic supplement ($n = 15$). Number of coexisted silicate and carbonate melt is also indicated if their compositions are available. *na* not available

Table 12 Representative compositions (wt. %) of quenched (after heating to 1,050°C) carbonate melt in melt inclusions hosted in perovskite, Kerimasi afrikandite, Trig Point Hill, Tanzania

No.	4	9	16	37	43	89	98	120	123	176	177	180	198	204	(n = 44)	
															Min	Max
SiO ₂	1.86	1.91	0.60	1.54	1.61	1.36	2.05	1.09	1.28	1.41	1.05	1.65	1.61	1.58	0.60	3.06
TiO ₂	0.58	0.31	0.33	0.42	0.69	0.50	0.54	0.42	0.37	0.36	0.21	0.40	0.56	0.44	0.21	0.69
Al ₂ O ₃	0.04	0.04	0.01	0.05	0.09	0.20	0.42	0.01	0.01	nd	0.03	0.19	0.01	0.26	0.01	0.42
FeO _T	1.43	1.06	1.69	1.57	1.01	0.84	1.25	1.05	0.82	0.72	0.96	1.86	1.33	2.04	0.39	2.77
MnO	0.28	0.17	0.31	0.35	0.25	0.18	0.21	0.20	0.15	0.76	0.22	0.29	0.34	0.21	0.15	0.76
NiO	nd	0.01	0.03	nd	0.01	0.02	nd	nd	nd	0.02	0.03	nd	nd	0.07	–	0.07
MgO	1.38	2.19	2.56	1.69	1.36	0.99	2.31	2.03	1.42	2.50	1.21	1.59	1.66	1.21	0.74	2.68
CuO	0.01	nd	0.02	nd	nd	0.06	nd	0.06	0.03	0.03	0.02	nd	nd	0.39	–	0.66
CaO	39.18	38.24	34.87	35.66	38.42	36.64	38.00	38.66	41.26	33.07	36.00	35.34	42.22	34.89	33.07	42.85
BaO	0.36	0.16	0.61	0.17	0.20	1.00	0.22	0.05	0.29	0.30	0.18	0.31	0.18	0.28	0.05	1.00
Na ₂ O	6.42	9.91	11.48	13.35	10.00	9.44	10.23	10.61	7.15	15.82	13.62	13.43	7.12	13.08	6.42	15.82
K ₂ O	7.09	6.92	6.22	4.92	6.33	8.71	5.61	5.89	6.91	5.67	6.17	5.33	5.20	4.65	4.34	8.71
P ₂ O ₅	5.00	4.29	5.22	4.03	4.81	3.89	5.08	4.21	4.29	3.78	4.10	4.49	6.51	5.16	3.05	7.26
F	0.38	0.77	0.51	0.11	0.73	0.28	0.77	0.61	0.30	0.82	0.50	0.14	1.46	0.36	0.07	1.91
SO ₃	0.26	0.33	0.40	0.21	0.09	0.14	0.05	0.17	0.14	0.17	0.75	0.27	0.09	1.12	0.05	1.65
Cl	0.01	nd	0.01	0.02	nd	nd	0.01	0.01	0.00	0.01	0.01	0.01	0.03	0.01	–	0.03
Total	64.25	66.31	64.85	64.07	65.60	64.26	66.74	65.07	64.41	65.43	65.04	65.31	68.30	65.74		

All the carbonate melts are coexisting with immiscible silicate melt

Note that all of studied quenched carbonate melt compositions in perovskite ($n = 44$) can be followed as electronic supplement. *nd* not detected, *FeO_T* all Fe expressed as FeO

immiscibility field, silicate liquidus surface and carbonate liquidus surface are also illustrated. Projected compositions as shown in Fig. 9a are enlarged in Fig. 9b to demonstrate the co-precipitation effects of nepheline and clinopyroxene on the compositions of the silicate melts hosted by perovskite, magnetite and nepheline. Compositional changes of the majority of the silicate melts reflect the co-precipitation of nepheline and clinopyroxene as the main

cause of melt evolution (gray arrows in Fig. 9b). However, most of the Mg- and Si-rich melt inclusions, found in the cores of perovskite and some nepheline (Fig. 7c), plot to the opposite side of the nepheline–clinopyroxene join on the [(CaO)–(SiO₂ + Al₂O₃ + TiO₂)–(Na₂O + K₂O)] plane (Fig. 9b). These compositions could represent those of the initial melts that were fractionated to give the major compositional trend as shown by the gray arrow in Fig. 9b,

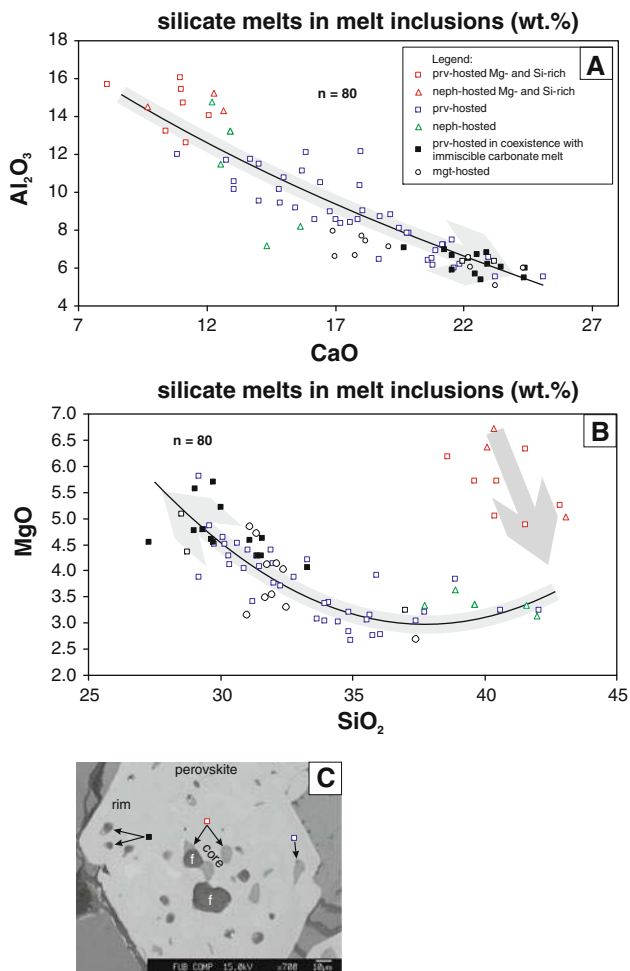


Fig. 7 Compositional variation of quenched silicate melts after heating to 1,050°C in melt inclusions hosted in perovskite, nepheline and magnetite, Kerimasi afrikandite, Tanzania. *Gray arrows* show the melt evolution that was mainly controlled by co-precipitation of nepheline and clinopyroxene. **b** Suggests that from the early melts (Mg- and Si-rich compositions) olivine also precipitated found in clinopyroxene megacrysts (see Fig. 2a). **c** Shows the distribution of the melt inclusions having different compositions in perovskite. Hole represents former fluid phase (f) that existed in the inclusions prior to exposure. *Mgt* magnetite, *Neph* nepheline, *Prv* perovskite

if a CaO-free and SiO₂-bearing phase, such as olivine, also precipitated at this time. This hypothesis is supported by the occurrence of olivine crystals in some of the clinopyroxene megacrysts (Fig. 2a). Fractionation of olivine at early stage of the melt evolution can connect the compositions of the Mg- and Si-rich silicate melt inclusions to the majority of silicate melt compositions in the MgO–SiO₂ plot (Fig. 7b).

The effects of melt evolution can also be seen by the variation in composition of the clinopyroxenes, which show a decrease in Al₂O₃ and TiO₂ (Fig. 6a) with increasing SiO₂ and MgO (Fig. 6b). This trend can be followed from the brown cores of megacryst to the green

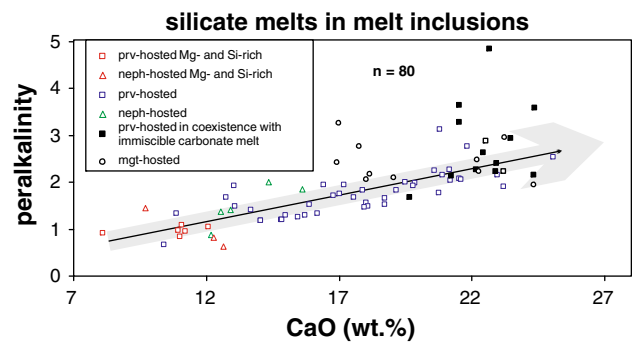


Fig. 8 Peralkalinity [(Na₂O + K₂O)/Al₂O₃, molar portions] versus CaO diagram showing the compositional variance in the quenched silicate melts after heating to 1,050°C in melt inclusions hosted in perovskite, nepheline and magnetite, Kerimasi afrikandite, Tanzania. *Gray arrows* show the melt evolution. Because the peralkalinity of nepheline and melilite is constant unity (0.98 and 1.03; Tables 3, 6, respectively), peralkalinity of the silicate melt could be increased by fractionation of clinopyroxene. The latter one shows significant decrease in Al₂O₃ (Fig. 6) at constant alkali content (Tables 1, 2)

rims (Fig. 1c); the latter have compositions similar to matrix clinopyroxenes (Fig. 6). The compositions of perovskite-hosted clinopyroxene inclusions overlap those of the brown cores and green rims of the clinopyroxene megacrysts (Fig. 6). These temporal and compositional relationships follow the silicate melt evolution trend. A decrease in Al₂O₃ is shown by all silicate melts (Fig. 7a). Both the clinopyroxenes and the silicate melts ultimately become slightly enriched in MgO (Figs. 6, 7) as a result of co-precipitation of the Mg-poor phases: nepheline, perovskite and magnetite. The silicate melts evolved from (SiO₂ + Al₂O₃)-rich to CaO-rich and (SiO₂ + Al₂O₃)-poor compositions (Figs. 7, 9).

Considering the low analytical total for all of the silicate melts, ranging between 89.1 and 97.8 wt. % (Tables 7, 8, 9, 10), it is probable that all of these silicate melts are carbonated. Enrichment of the melt in carbonate during evolution could result from fractionation of the carbonate-free major minerals. It should be noted that similar low analytical total have been reported in previous studies of silicate melt inclusions coexisting with carbonate melt inclusions in perovskite from the Gardiner Complex (Nielsen et al. 1997), in silicate glass in silicate–carbonate melt inclusions in nepheline from Oldoinyo Lengai (Mitchell 2009) and in experimentally produced quenched silicate melt coexisting with carbonate melt (Kjarsgaard 1998).

Comparison with experimental data

On the basis of the quenched melt and rock-forming mineral compositions together with phase relationships in the model haplocarbonatite system (Lee and Wyllie 1998), it is probable that at an early stage of the melt evolution a

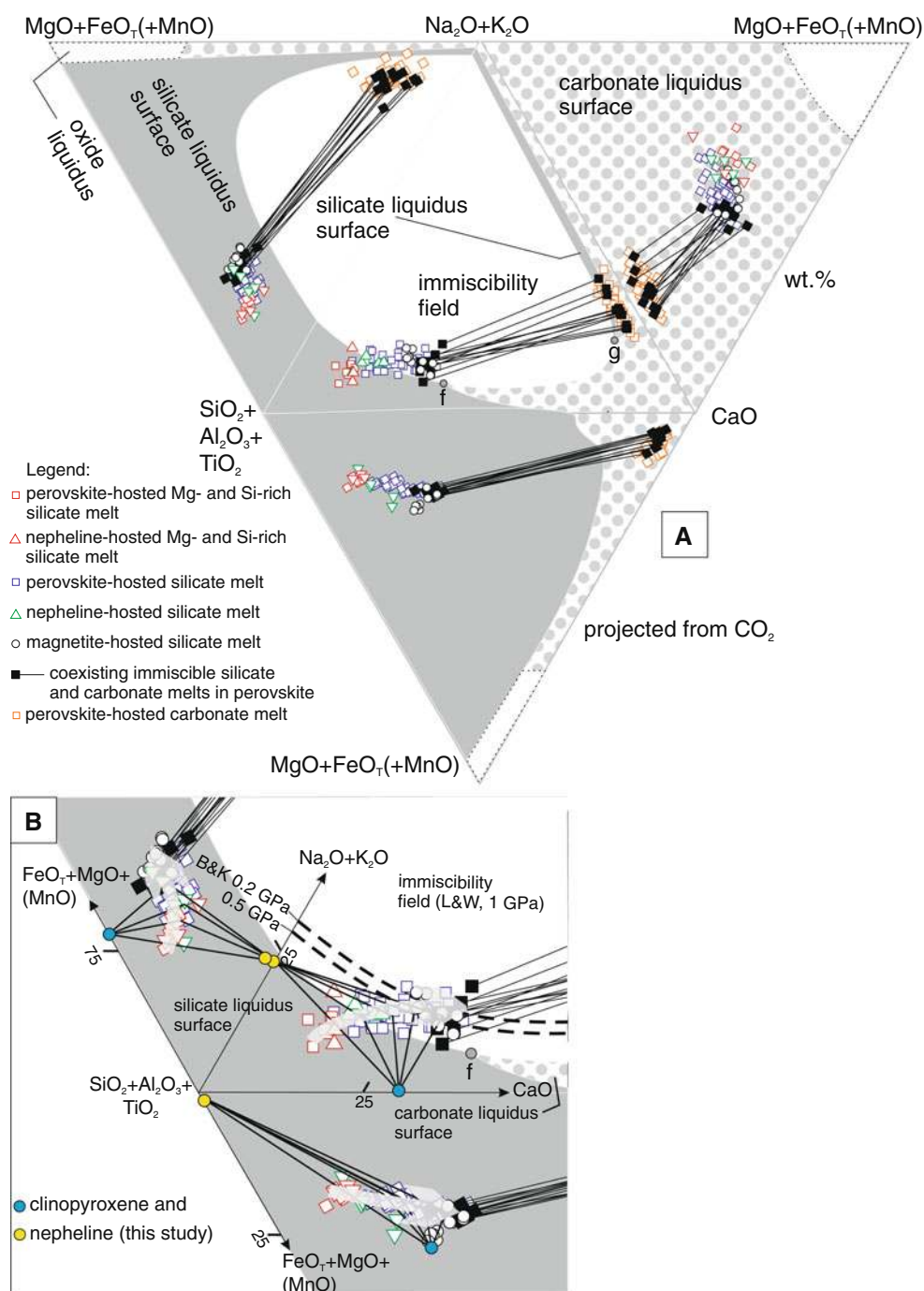


Fig. 9 Quenched melts ($n = 138$) after heating to 1,050°C in melt inclusions of perovskite, nepheline and magnetite, plotted in the pseudo-quaternary diagram [(CaO)–(MgO + FeO_T)–(SiO₂ + Al₂O₃ + TiO₂)–(Na₂O + K₂O)] projected from CO₂ (Lee and Wyllie 1998, L&W), showing the silicate liquidus surface, the carbonate liquidus surface, together with the immiscibility field (1 GPa). Points f and g are in the intersections of these surfaces on the (FeO^T + MgO + MnO)-free plane. Immiscibility fields determined at 0.2 and 0.5 GPa by Brooker and Kjarsgaard (2010, B&K) for the system [Na₂O–(SiO₂ + Al₂O₃)–CaO] is also shown. Arrows illustrate the

compositional evolution of the perovskite-, nepheline- and magnetite-hosted melts. The presented chemical evolution led up immiscibility between the silicate and carbonate melts. **b** Shows an enlarged part of **a**, indicating that the melt evolution, recorded by the quenched silicate melts in perovskite, magnetite and nepheline, was principally determined by co-precipitation of the main rock-forming phases, such as the nepheline and clinopyroxene. Note that MnO is only in our system. Uncertainties are smaller than the symbols used. FeO_T—all Fe as FeO. For further details see the text

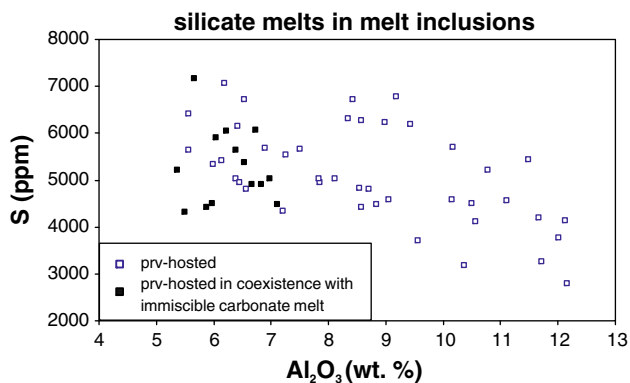


Fig. 10 Sulfur versus alumina diagram showing compositional variation of quenched silicate melt after heating to 1,050°C in perovskite-hosted melt inclusions

carbonated and fluid-saturated alkaline-rich silicate melt existed. This melt could have been a carbonated nephelinitic magma, the earliest melts in Figs. 7 and 9 (Table 7), from which nepheline, diopside, olivine and perovskite precipitated. The initial composition was in the silicate liquidus field (Fig. 9), and changes in the melt composition were mainly determined by co-precipitation of nepheline and clinopyroxene. This resulted in CaO (Figs. 7, 9), sulfur (Fig. 10) and carbonate enrichment in the fractionated melt. Precipitation of melilite and magnetite also occurred; however, their effect on melt compositional changes is not as clearly demonstrated as that of clinopyroxene and nepheline. Peralkalinity [molar $(\text{Na}_2\text{O} + \text{K}_2\text{O})/\text{Al}_2\text{O}_3$] of the silicate melt also increased from ~ 1 to 3 (Fig. 8). Because the peralkalinity of nepheline (0.98 on average, Table 3) and melilite (1.03 on average, Table 6) is close to unity, fractionation of these minerals will have no effect on melt peralkalinity. The melt peralkalinity could be increased by fractionation of clinopyroxene (its peralkalinity varies from 0.2 to 2.1), that is, removal of Al_2O_3 (Fig. 6) at a constant alkali content (Tables 1, 2). Ultimately, silicate melt compositions reached the immiscibility field boundary and split into immiscible silicate and carbonate melts (conjugated black and gray squares in Fig. 9 and 11, respectively). At this time, the immiscible melt compositions also changed within the tetrahedron (Figs. 9, 11) along two lines, according to the boundaries of three volumes: silicate liquidus, carbonate liquidus and immiscible compositions. This allowed crystallization of both silicates (nepheline, clinopyroxene and melilite) and carbonate (calcite) (Fig. 1f) during the evolution of the immiscible melts. We consider that the evolutionary trends depicted in Figs 9 and 11 could have produced carbonate melts with compositions similar to those that could have produced Kerimasi calciocarbonatite rock (Fig. 11). Thus, the carbonate melt could be physically separated from

the silicate melt and transported to lower pressures and temperatures, eventually to become the parental melt of Kerimasi calciocarbonatite and, ultimately, to natrocarbonatite (Fig. 11). The rare occurrence of sulfide melts in magnetite compared to those in perovskite suggests that sulfide melt could also separate during melt(s) evolution. In contrast to carbonate melt, sulfide melt would probably sink due to its higher density than that of the silicate melt (Mungall 2002; Holzheid 2010).

To estimate the pressure at which immiscibility occurred, we show in Fig. 9b the silicate–carbonate immiscibility fields determined at 0.2 and 0.5 GPa in the system $[(\text{CaO})-(\text{SiO}_2 + \text{Al}_2\text{O}_3)-(\text{Na}_2\text{O})-(\text{CO}_2)]$ by Brooker and Kjarsgaard (2010). On the $[(\text{CaO})-(\text{SiO}_2 + \text{Al}_2\text{O}_3 + \text{TiO}_2)-(\text{Na}_2\text{O} + \text{K}_2\text{O})]$ plane, the compositions of our silicate melts coexisting with immiscible carbonate melts (connected black squares) are closer to the limb of immiscibility field determined at 0.2 GPa pressure (Brooker and Kjarsgaard, 2010) than those determined at higher pressure (Lee and Wyllie 1998, 1 GPa). Our analyzed melts contain significant amounts of FeO_T and MgO , (Figs. 9, 11; Tables 7, 8, 9, 10), which lead to a decrease in the size of the immiscibility field relative to that determined in the $[\text{FeO}_T + \text{MgO} + \text{MnO}]$ -free plane, regardless of pressure (e.g., Lee and Wyllie 1998, 1 GPa) (Fig. 9 in this study). Therefore, higher pressures than 0.2 GPa seem to be probable for the immiscibility recorded by our melt inclusions in perovskite. We estimated the pressure values to be between 0.5 and 1 GPa, based on Figs. 9 and 11.

Distribution of major elements between immiscible silicate and carbonate melts

On the basis of the compositions of coexisting silicate and carbonate melts in the quenched melt inclusions in perovskite (Table 10), the distribution of major elements between silicate and carbonate melts ($D_{\text{SIL-CARB}}$) has been calculated (Fig. 12). Sodium ($D_{\text{SIL-CARB}} = 0.51\text{--}0.98$), K (0.26–0.72), Ca (0.48–0.75), P (0.26–0.68) and F (0.08–0.33) were partitioned into carbonate melt, whereas Mg ($D_{\text{SIL-CARB}} = 1.92\text{--}4.61$), Mn (2.37–8.82), Fe_T (7.27–18.43), Al (30.6–364), Si (15.1–23.8), Ti (3.10–8.89) and S (4.72–22.9) are concentrated in the silicate melt. The distribution is quite similar (Fig. 12) to that reported for other coexisting immiscible melts (Kjarsgaard 1998; Mitchell 2009). Significant differences have been observed with respect to sulfur (Fig. 12) and to potassium. Sulfur is compatible with the silicate melt phase in this study, but incompatible to silicate melts analyzed by Mitchell (2009), although these latter melts have more evolved compositions and lower temperatures of formation (700–750°C, Fig. 13) than the melts studied here. Furthermore, melts studied by Mitchell (2009) are hosted by nepheline

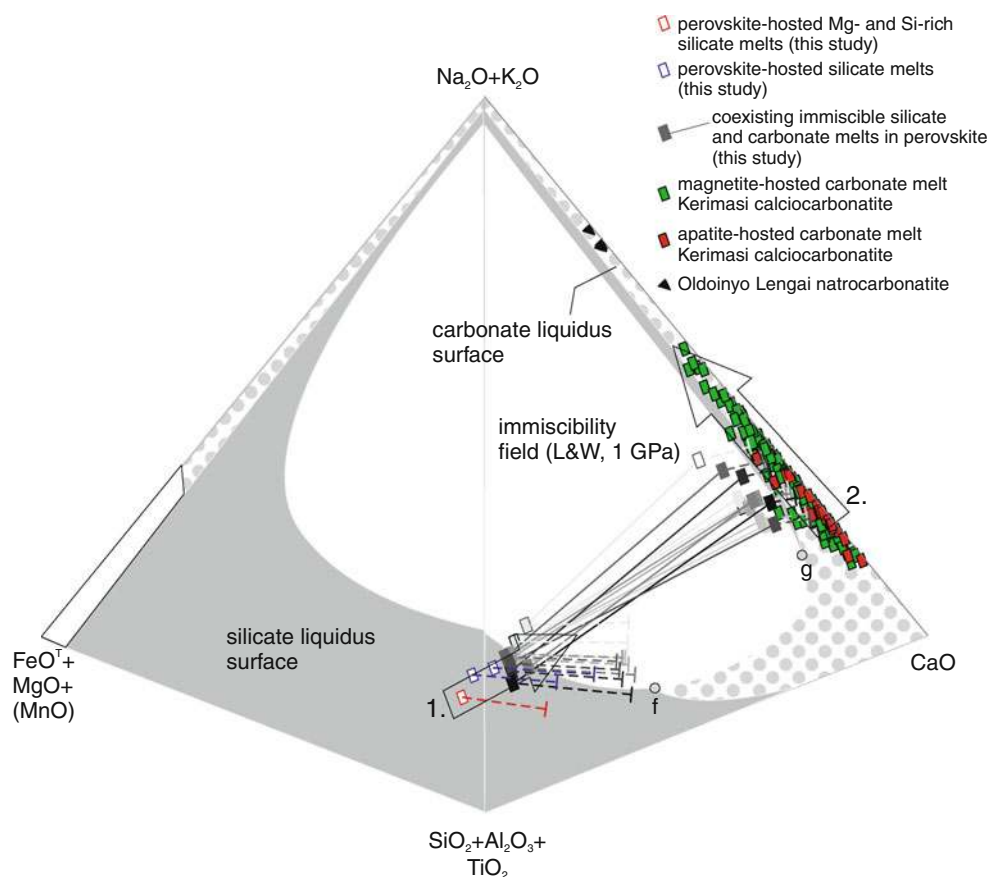


Fig. 11 Evolution of the studied melts shown in tetrahedron that was drawn from Fig. 9a. Phase fields are the same as on Fig. 9a determined by Lee and Wyllie (1998) at 1 GPa (L&W). Representative composition of the quenched perovskite-hosted silicate melts and that of the coexisting silicate and carbonate melts are plotted inside the tetrahedron. For comparison, compositions of carbonate melt inclusions of Kerimasi calciocarbonatite (Guzmics et al. 2011) and that of Oldoinyo Lengai natrocarbonatite (Dawson et al. 1990, 1996) also plotted, but on the $(\text{FeO}_T + \text{MgO} + \text{MnO})$ -free plane because of their low $(\text{MgO} + \text{FeO}_T)$ -content relative to melts in this study. *Arrow-1* shows the melt evolution in this study, whereas

arrow-2 does for Kerimasi calciocarbonatite. *Dotted lines* are projections of composition of the perovskite-hosted silicate melts onto the $[(\text{Na}_2\text{O} + \text{K}_2\text{O})-(\text{SiO}_2 + \text{Al}_2\text{O}_3 + \text{TiO}_2)\text{-CaO}]$ plane of tetrahedron. According to observed compositional change in the studied melts, Ca-rich carbonate melt could separate from our studied system with similar composition to melts of Kerimasi calciocarbonatite, suggesting their genetic relation. Evolution of the carbonated nephelinite melt (e.g., *open red diamond*) could lead up natrocarbonatite compositions through Ca-rich carbonate melt compositions, precipitating firstly afrikandite rock by the silicate melt (*Arrow-1*) and then calciocarbonatite rock by the separated carbonate melt (*Arrow-2*)

phenocrysts from an erupted ash, in contrast to the plutonic melt inclusions investigated in this work. These observations suggest that the melt system studied by Mitchell (2009) is more oxidized than that studied here. Thus, the differences in sulfur distribution between the two investigations might be a consequence of the differing behavior of S in oxidized systems (e.g., as SO_4^{2-}) relative to that of sulfide (e.g., as S^{2-}) [Carroll and Rutherford, 1985; Clemente et al. 2004]. Potassium is compatible with the carbonate melt phase in this study, but incompatible to carbonate melts analyzed by Mitchell (2009). This can also be resulted in difference in chemistry of the bulk melt system together with temperature and pressure of formation of immiscibility between the two studies.

Why are most of carbonatites calciocarbonatite?

The majority of carbonatites are calcium-rich (calciocarbonatite, sövite, alvikite) compositions rather than dolomitic (rauhaugite and before-site) or sideritic types (Heinrich 1966; Tuttle and Gittins 1966; Le Bas 1977; Bell 1989; Mitchell 2005; Wooley and Kjarsgaard 2008). Our studies of numerous natural silicate and carbonate melts show significant enrichment of Ca, P and F relative to Mg, Fe_T , Mn, Al, Si and Ti in the immiscible carbonate melt (Figs. 9, 11, 12). We have additionally shown that this is the case even when the silicate parent of the immiscible carbonate melt is MgO- and FeO_T -rich, and immiscible sulfide melt is also present (Figs. 4, 5). It is clear that after

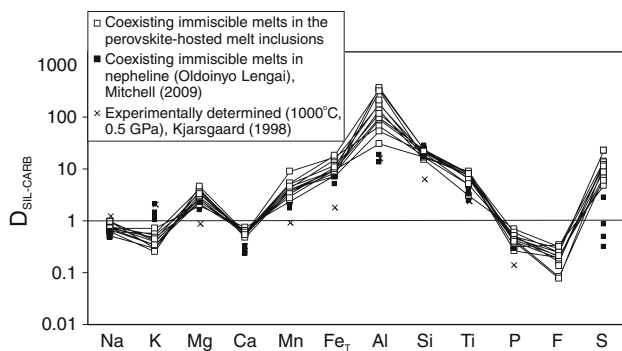


Fig. 12 Calculated distributions for major element between coexisting immiscible silicate and carbonate melts in the quenched (after heating to 1,050°C) perovskite-hosted melt inclusions. Strong partitioning of Ca, P and F relative to Fe_T, Si, Al, Mn, Ti and Mg in the carbonate melt explains Ca-rich nature of the immiscible carbonate melt. Natural observations (in nepheline-hosted melt inclusions; Mitchell 2009) and experimental results (on carbonated nephelinite; Kjarsgaard 1998) are shown for comparison. For further details see the text. Fe_T—all Fe as FeO

physical separation of a CaCO₃-rich (and alkali-bearing) carbonatite magma, such as the carbonate melts described here (Figs. 9, 12), it can precipitate calcite, that is, form a calciocarbonatite rock (Lee and Wyllie 1997; Kjarsgaard 1998). In our interpretation, in agreement with experimental (Kjarsgaard 1998) and our previous work (Guzmics et al. 2011), the dominance of calciocarbonatites could result from calcite fractionation from such immiscible carbonate magmas. Continued fractionation of calcite will enrich the residual magma in alkalis and could eventually produce small volumes of natrocarbonatite (Guzmics et al. 2011).

Possible source of the parent silicate melt and significance of immiscible sulfide melt

The Mg- and Si-rich melt inclusions found in the perovskite and nepheline (Figs. 7, 9, 11) are interpreted as the most primitive melts in composition of those analyzed in this work and are essentially carbonated nephelinitic compositions (Table 7). This type of magma can be derived from an enriched (metasomatized) mantle that has some trace of carbonate (King and Sutherland 1960; Wyllie and Huang 1976; Egglar 1978; Lee and Wyllie 1998; references therein). We have shown above that with the evolution of the silicate melt composition (Figs. 7, 9, 10), in addition to carbonate immiscibility, saturation with respect to sulfur was also attained resulting in formation of sulfide melt phase (Figs. 4, 5). This sulfide melt is extremely low in Ni (up to 0.2 wt. %) (Table 11) compared to most sulfide melts formed at the onset of basalt–sulfide–liquid immiscibility or exist in ultrabasic systems (Andersen et al. 1987; Flet and Stone 1990; Szabó and Bodnar

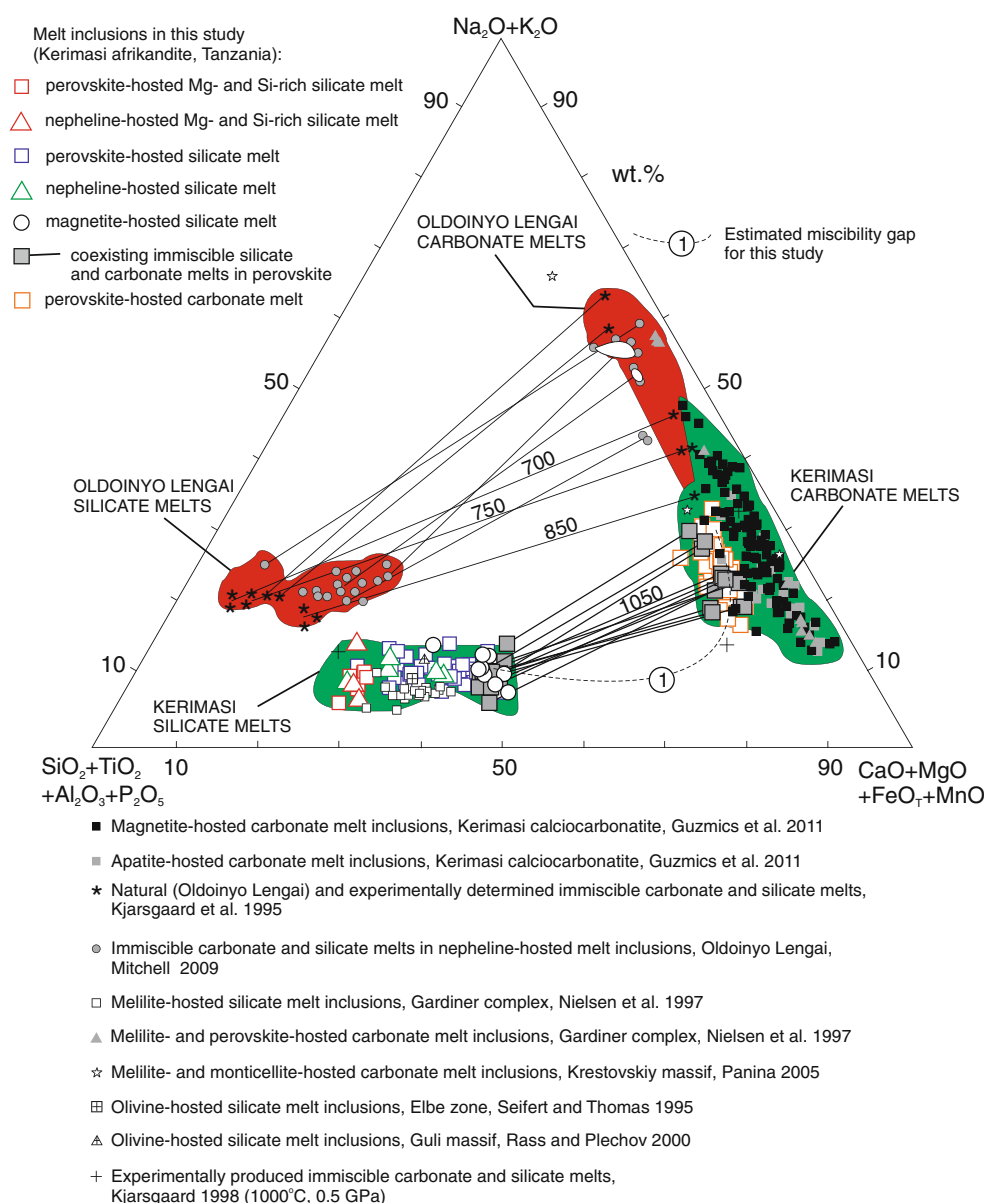
1995). As noted above, olivine fractionation could have occurred prior to melt entrapment in the early perovskite and nepheline. However, it is difficult to establish what process [e.g., relatively low degree of partial melting of an enriched mantle and/or fractionation process] could result in such a Ni-poor silicate melt that exsolved a sulfide melt containing almost no Ni (Table 11). The Fe–Cu–S melt compositions (Table 11) could be characteristic of sulfide melts originating by immiscibility from carbonated nephelinitic magmas. In this respect, economically significant copper sulfide deposits occur in alkaline silicate–carbonatite complexes, for example, the Phalabowra complex, South Africa (Groves and Vielreicher 2001) and the Salmagorskii complex, Kola Peninsula (Korobeinikov et al. 1998). Although no such deposit has been discovered at Kerimasi, our melt inclusion data (Figs. 7, 8, 9, 11) suggest that the parental melts of alkaline silicate–carbonatite complexes are capable of carrying large amounts of sulfur (Fig. 10) that could be separated as immiscible sulfide melts (Figs. 4, 5) and, ultimately form Cu–Fe sulfide deposits. Our work shows that without studying melt inclusions in the afrikandite, the existence of a sulfide melts would have not been recognized, demonstrating the significance of detailed studies of melt inclusions.

Comparison with previous melt inclusion studies of alkaline silicate–carbonatite complexes

Previous studies have reported natural examples of quenched coexisting carbonate and silicate melt inclusions in silicate and carbonatite rocks from various localities (Fig. 13) hosted by (1) melilite and perovskite (Nielsen et al. 1997; melilitolite, Gardiner complex); (2) melilite and monticellite (Panina 2005; olivine melilitite, Krestovskiy massif); (3) olivine (Seifert and Thomas 1995; olivine melilitite, Elba zone; Rass and Plechov 2000; olivine melilitite, Guli complex); (4) apatite and magnetite (Guzmics et al. 2011; calciocarbonatite; Kerimasi). Although none of these studies demonstrated melt evolution from a carbonated nephelinite by immiscibility to a Ca-rich and eventually natro-carbonate melt, the compositional similarities between our studied silicate melts and those noted above (Fig. 13) suggest that a common evolutionary process, which includes silicate–carbonate immiscibility, has occurred at all of these alkaline silicate–carbonatite complexes.

In a comparison of the melt inclusions from Kerimasi and Oldoinyo Lengai, it is evident that the carbonate melt compositions overlap (Fig. 13). Generally, carbonate melts at Oldoinyo Lengai are more evolved, richer in alkalis and have lower formation temperatures than melts at Kerimasi (Fig. 13). Silicate melts from Kerimasi are rich in CaO and MgO relative to strongly peralkaline combeite wollastonite nephelinite melts from Oldoinyo Lengai and are essentially carbonated melilite nephelinites (Fig. 13). These data show

Fig. 13 Hamilton projection (Hamilton et al. 1979) of the quenched silicate and carbonate melts ($n = 138$) in the melt inclusions hosted in co-precipitated perovskite, nepheline and magnetite. All of studied carbonate melts coexist with silicate melt. For comparison, composition of natural immiscible carbonate and silicate melt inclusions, as well as experimental data, are also plotted. *Tie-lines* connect the conjugate silicate–carbonate compositions in this study and that studied by Kjarsgaard et al. (1995) and by Mitchell (2009). *Numbers on the lines* show temperatures (in °C) determined in this study and also by Kjarsgaard et al. (1995)



that diverse carbonated silicate magmas are all capable of producing natrocarbonatite melts.

Conclusion

On the basis of homogenization experiments, temperatures are estimated to be 1,100°C for the early stage of the melt evolution of the magma forming Kerimasi afrikandite. At that time, a carbonated nephelinitic magma existed, which was probably formed by partial melting of a carbonate-bearing mantle. The compositional evolution of this melt was determined by study of a statistically significant number of melt inclusions, entrapped in coprecipitated perovskite, nepheline and magnetite. The magma became

enriched in CaO and depleted in SiO₂ and Al₂O₃. This compositional change was controlled principally by coprecipitation of nepheline and clinopyroxene. Melt evolution resulted in immiscibility of three fluid-saturated melts: an alkali- and MgO-bearing, CaO- and FeO-rich silicate melt; an alkali- and F-bearing, CaO-, P₂O₅-rich carbonate melt; and a Cu-Fe sulfide melt at ~1,050°C and crustal pressures (0.5–1 GPa). Cu–Fe–S melt compositions are characteristic of sulfide melts originating by immiscibility from the parental silicate melts of alkaline silicate–carbonatite complexes. The distribution of major elements between perovskite-hosted coexisting immiscible silicate and carbonate melts show strong partitioning of Ca, P and F relative to Fe_T, Si, Al, Mn, Ti and Mg in the carbonate melt, indicating that immiscibility occurring at crustal

pressures can be the responsible for the dominance of calciocarbonatite rocks over Mg- and Fe-rich carbonatites. The Kerimasi carbonated nephelinite parent magma exsolved an immiscible calcium-rich carbonate magma. Low-temperature natrocarbonatite magmas can be formed by calcite fractionation from a calcium-rich carbonate magma (as at Kerimasi) or immiscibility from an evolved strongly peralkaline nephelinite magma (as at Oldoinyo Lengai).

Acknowledgments This project was financially supported by the European Union and co-financed by the European Social Fund (grant agreement number: TAMOP 4.2.1/B-09/1/KMR-2010-0003 to Tibor Guzmics and Csaba Szabó). T. Guzmics was additionally supported by the János Bolyai Research Scholarship of the Hungarian Academy of Sciences. T. Guzmics thanks the Hungarian Science Foundation (OTKA, 78425 to Cs. Szabó). Roger Mitchell's work on alkaline rocks is supported by the Natural Sciences and Engineering Council of Canada, Almaz Petrology and Lakehead University. The authors owe thanks to Zsolt Bendő and Gábor Varga at Eötvös University and to Gerlinde Habler at University of Vienna for the help in SE and BSE imaging. The authors are also grateful to Professor Jacques Touret and an anonymous reviewer for their constructive reviews and useful suggestions. This is publication No 57 of Lithosphere Fluid Research Laboratory, Eötvös University, Budapest. This work is dedicated to Tibor Guzmics Sr.

References

- Andersen T, Griffin WL, O'Reilly SY (1987) Primary sulfide melt inclusions in mantle derived phenocrysts and pyroxenites. *Lithos* 20:279–294
- Bailey DK (1993) Carbonatite magmas. *J Geol Soc London* 150:637–651
- Bell K (ed) (1989) Carbonatites: genesis and evolution, Unwin Hyman, London
- Bodnar RJ, Student JJ (2006) Melt inclusions in plutonic rocks: petrography and microthermometry. In: Webster JD (ed) Melt inclusions in plutonic rocks, vol 36. Mineralogical Association of Canada Short Course, Canada, pp 1–25
- Brooker RA, Kjarsgaard BA (2010) Silicate–carbonate liquid immiscibility and phase relations in the system $\text{SiO}_2\text{--Na}_2\text{O--Al}_2\text{O}_3\text{--CaO--CO}_2$ at 0.1–2.5 GPa with applications to carbonatite genesis. *J Petrol* 52:1281–1305
- Carroll MR, Rutherford MJ (1985) Sulphide and sulfate saturation in hydrous silicate melts. *J Geophys Res* 90:C601–C612
- Clemente B, Scaillet B, Pichavant M (2004) The solubility of sulphur in hydrous rhyolitic melts. *J Petrol* 45:2171–2196
- Danyushevsky LV, McNeil AW, Sobolev AV (2002) Experimental and petrological studies of melt inclusions in phenocrysts from mantle-derived magmas: an overview of techniques, advantages and complications. *Chem Geol* 183:5–24
- Dawson JB, Pinkerton H, Norton GE, Pyle DM (1990) Physicochemical properties of alkali carbonatite lavas: data from the 1988 eruption of Oldoinyo Lengai, Tanzania. *Geology* 18:260–263
- Dawson JB, Pinkerton H, Pyle DM, Nyamweru C (1994) June 1993 eruption of Oldoinyo Lengai, Tanzania: exceptionally viscous and large carbonatite lava flows and evidence for coexisting silicate and carbonate magmas. *Geology* 22:799–802
- Dawson JB, Pyle DM, Pinkerton H (1996) Evolution of natrocarbonatite from a wollastonite nephelinite parent: evidence from the June 1993 eruption of Oldoinyo Lengai, Tanzania. *J Geol* 104:41–54
- Eggler DH (1978) The effect of CO_2 upon partial melting peridotite in the system $\text{Na}_2\text{O--CaO--Al}_2\text{O}_3\text{--MgO--SiO}_2\text{--CO}_2$ to 35 kb, with an analysis of melting in a peridotite– $\text{H}_2\text{O--CO}_2$ system. *Am J Sci* 278:305–343
- Flet ME, Stone WE (1990) Nickeliferous sulfides in xenoliths, olivine phenocrysts and basaltic glass. *Contrib Mineral Petrol* 105:629–636
- Groves DI, Vielreicher MN (2001) The Phalabowra (Palabora) carbonatite-hosted magnetite-copper sulfide deposit, South Africa: an end member of the iron-oxide copper-gold–rare earth element deposit group? *Mineral Deposit* 36:189–194
- Guzmics T, Zajacz Z, Kodolányi J, Werner H, Szabó C (2008) LA-ICP-MS study of apatite- and K-feldspar-hosted primary carbonatite melt inclusions in clinopyroxenite xenoliths from lamprophyres, Hungary: implication for significance of carbonatite melts in the Earth's mantle. *Geochim Cosmochim Acta* 72:1864–1886
- Guzmics T, Mitchell RH, Szabó Cs, Berkesi M, Milke R, Abart R (2011) Carbonatite melt inclusions in coexisting magnetite, apatite and monticellite in Kerimasi calciocarbonatite, Tanzania: melt evolution and petrogenesis. *Contrib Mineral Petrol* 161:177–196
- Hamilton DL, Freestone IC, Dawson JB, Donaldson CH (1979) Origin of carbonatites by liquid immiscibility. *Nature* 279:52–54
- Haughton DR, Roeder PL, Skinner BJ (1974) Solubility of sulfur in mafic magmas. *Econ Geol* 69:451–467
- Hay RL (1983) Natrocarbonatite tefra of Kerimasi volcano, Tanzania. *Geology* 11:599–602
- Heinrich EW (1966) The geology of carbonatites. Rand McNally, Chicago 555 p
- Hidas K, Guzmics T, Szabó Cs, Kovács I, Bodnar RJ, Zajacz Z, Nédli Zs, Vaccari L, Perucchi A (2010) Coexisting silicate melt inclusions and H_2O -bearing, CO_2 -rich fluid inclusions in mantle peridotite xenoliths from the Carpathian-Pannonian region (central Hungary). *Chem Geol* 274:1–18
- Holzheid A (2010) Separation of sulfide melt droplets in sulfur saturated silicate liquids. *Chem Geol* 274:127–135
- King BC, Sutherland DL (1960) Alkaline rocks of eastern and southern Africa. *Sci Prog* 47:298–321, 504–521, 709–720
- Kjarsgaard BA (1998) Phase relations of a carbonated high CaO nephelinite at 0.2 and 0.5 GPa. *J Petrol* 39:2061–2075
- Kjarsgaard BA, Peterson TD (1991) Nephelinite-carbonatite liquid immiscibility at Shombole volcano, East Africa: petrographic and experimental evidence. *Mineral Petrol* 43:293–314
- Kjarsgaard BA, Hamilton DL, Peterson TD (1995) Peralkaline nephelinite/carbonatite liquid immiscibility: comparison of phase compositions in experiments and natural lavas from Oldoinyo Lengai. In: Bell K, Keller J (eds) Carbonatite volcanism. Springer, Berlin, pp 163–190
- Kogarko LN, Plant DA, Henderson CMB, Kjarsgaard BA (1991) Na-rich carbonate inclusions in perovskite and calzirtite from the Guli intrusive Ca-carbonatite, polar Siberia. *Contrib Mineral Petrol* 109:124–129
- Kogarko LN, Kurat G, Ntaffos T (2001) Carbonate metasomatism of the oceanic mantle beneath Fernando de Noronha Island, Brazil. *Contrib Mineral Petrol* 140:577–587
- Korobeinikov AN, Mitrofanov FP, Gehör S, Laajoki K, Pavlov VP, Mamontov VP (1998) Geology and copper sulphide mineralization of the Salmagorskii Ring igneous complex, Kola Peninsula, NW Russia. *J Petrol* 39:2033–2041
- Koster van Groos AF, Wyllie PJ (1968) Liquid immiscibility in the join $\text{NaAlSi}_3\text{O}_8\text{--Na}_2\text{CO}_3\text{--H}_2\text{O}$. *Am J Sci* 266:932–967
- Le Bas MJ (1977) Carbonatite-nephelinite volcanism. Wiley, London 347 p

- Le Bas MJ, Aspden JA (1981) The comparability of carbonatitic fluid inclusions in ijolites and natrocarbonatite lava. *Bull Volcan* 44:429–438
- Lee W-J, Wyllie PJ (1997) Liquid immiscibility in the join $\text{NaAlSi}_3\text{O}_8\text{--NaAlSi}_3\text{O}_8\text{--CaCO}_3$ at 1 GPa: Implications for crustal carbonatites. *J Petrol* 38:1113–1135
- Lee W-J, Wyllie PJ (1998) Petrogenesis of Carbonatite Magmas from Mantle to Crust, Constrained by the System $\text{CaO--(MgO + FeO*)--(Na}_2\text{O + K}_2\text{O)--(SiO}_2\text{ + Al}_2\text{O}_3\text{ + TiO}_2\text{)--CO}_2$. *J Petrol* 39:495–517
- Li C, Ripley EM (2005) Empirical equations to predict the sulfur content of mafic magmas at sulfide saturation and applications to magmatic sulfide deposits. *Mineral Deposit* 40:218–230
- Liu Y, Samaha N-T, Baker DR (2007) Sulfur concentration at sulfide saturation (SCSS) in magmatic silicate melts. *Geochim Cosmochim Acta* 71:1783–1799
- Mavrogenes JA, O'Neill H (1999) The relative effects of pressure, temperature and oxygen fugacity on the solubility of sulfide in mafic magmas. *Geochim Cosmochim Acta* 63:1173–1180
- Mitchell RH (2005) Carbonatites and carbonatites and carbonatites. *Can Mineral* 43:1852–1853
- Mitchell RH (2009) Peralkaline nephelinite-natrocarbonatite immiscibility and carbonatite assimilation at Oldoinyo Lengai, Tanzania. *Contrib Mineral Petrol* 158:589–598
- Mungall JE (2002) Kinetic controls on the partitioning of trace elements between silicate and sulfide liquids. *J Petrol* 43:749–768
- Naldrett AJ (1989) *Magmatic sulfide deposits*. Oxford University Press, Oxford
- Nielsen TFD (1980) The petrology of a melilitolite, melteigite, carbonatite and syenite ring dike system in the Gardiner complex, East Greenland. *Lithos* 13:181–197
- Nielsen TFD, Solovova IP, Veksler IV (1997) Parental melts of melilitolite and origin of alkaline carbonatite: evidence from crystallised melt inclusions, Gardiner complex. *Contrib Mineral Petrol* 126:331–344
- O'Neill H, Mavrogenes JA (2002) The sulfide capacity and the sulfur content at sulfide saturation of silicate melts at 1400°C and 1 bar. *J Petrol* 43:1049–1087
- Panina LI (2005) Multiphase carbonate-salt immiscibility in carbonatite melts: data on melt inclusions from the Krestovskiy massif minerals (Polar Siberia). *Contrib Mineral Petrol* 150:19–36
- Panina LI, Stoppa F (2009) Silicate-carbonate-salt liquid immiscibility and origin of the sodalite-haüyne rocks: study of melt inclusions in olivine foidite from Vulture volcano, S Italy. *Cent Eur J Geosci* 1:377–392
- Poulson SR, Ohmoto H (1990) An evaluation of the solubility of sulfide sulfur in silicate melts from experimental data and natural samples. *Chem Geol* 85:57–75
- Rass IT, Plechov PY (2000) Melt inclusions in olivines of olivine-melilitite rocks, Guli Massif, northwest of the Siberian Platform. *Dokl Earth Sci* 375:389–392
- Ripley EM, Brophy JG, Li C (2002) Copper solubility in a basaltic melt and sulfide liquid/silicate melt partition coefficients of Cu and Fe. *Geochim Cosmochim Acta* 66:2791–2800
- Roedder E (1984) Fluid inclusions. In: Ribbe PH (ed) *Reviews in mineralogy*, vol 12. Mineralogical Society of America Series, Chelsea, p 646
- Roedder E (1987) Silicate liquid immiscibility in magmas. In: Yoder HS (ed) *The evolution of the igneous rocks*. Princeton University Press, Princeton, pp 15–58
- Roedder E (1992) Fluid inclusion evidence for immiscibility in magmatic differentiation. *Geochim Cosmochim Acta* 56:5–20
- Seifert W, Thomas R (1995) Silicate-carbonate immiscibility: a melt inclusion study of olivine melilitite and wehrilite xenoliths in tephrite from the Elbe Zone, Germany. *Chem Erde* 55:263–279
- Sokolov SV, Veksler IV, Senin VG (1999) Alkalis in carbonatite magmas: new evidence from melt inclusions. *Petrology* 7:602–609
- Solovova IP, Giris AV, Ryabchikov ID, Simakin SG (2006) High-temperature carbonatite melt and its interrelations with alkaline magmas of the Dunkel'dyk complex, southeastern Pamirs. *Dokl Earth Sci* 410:1148–1151
- Szabó C, Bodnar RJ (1995) Chemistry and origin of mantle sulfides in spinel peridotite xenoliths from alkaline basaltic lavas, Nógrád-Gömör volcanic field, northern Hungary and southern Slovakia. *Geochim Cosmochim Acta* 59:3917–3927
- Tuttle OF, Gittins J (1966) *Carbonatites*. Interscience, New York 591 p
- Veksler IV (2006) Crystallized melt inclusions in gabbroic rocks. In: Webster JD (ed) *Melt inclusions in plutonic rocks*, vol 36. Mineralogical Association of Canada Short Course, Canada, pp 99–122
- Veksler IV, Lentz D (2006) Parental magmas of plutonic carbonatites, carbonate-silicate immiscibility and decarbonation reactions: evidence from melt and fluid inclusions. In: Webster JD (ed) *Melt inclusions in plutonic rocks*, vol 36. Mineralogical Association of Canada Short Course, Canada, pp 123–150
- Wooley AR, Kjarsgaard BA (2008) Carbonatite occurrences of the world: map and database; geological survey of Canada, Open file 5796, 1 CD-ROM + 1 map
- Wyllie PJ, Huang W-L (1976) Carbonation and melting reactions in the system $\text{CaO--MgO--SiO}_2\text{--CO}_2$ at mantle pressures with geophysical and petrological applications. *Contrib Mineral Petrol* 54:79–107